

# Unobserved Heterogeneity in Threshold Regression Based on the Hitting Times of a Reflected Brownian Motion for Recurrent Hypoglycemia

Yingfa Xie<sup>1,3</sup>, Haoda Fu<sup>2</sup>, Yuan Huang <sup>\*3</sup> and Jun Yan<sup>1</sup>

<sup>1</sup>*Department of Statistics, University of Connecticut*

<sup>2</sup>*Indiana University School of Medicine*

<sup>3</sup>*Department of Biostatistics, Yale School of Public Health*

## Abstract

Analyses of recurrent hypoglycemia are critical for effective treatment management in diabetic patients. Typically, within-subject dependency in such analyses is captured through subject-level frailty. Recent research has modeled recurrent hypoglycemia using the first hitting times of a reflected Brownian motion. A close examination of this approach reveals that it does not adequately account for varying frailties among individuals, which indicate notable heterogeneity. To address this gap, we propose a finite mixture model of the first hitting time distribution of the reflected Brownian motion. This model allows for component-specific regression coefficients and frailty parameters, providing nuanced insights into how risk factors differently affect patient subgroups. We employ a Bayesian framework for inference, utilizing Markov chain Monte Carlo for estimation. Model selection is conducted using the Deviance Information Criterion and the Logarithm of the Pseudo-Marginal Likelihood. The effectiveness of these criteria is assessed through simulation studies. Application to recurrent hypoglycemia modeling revealed two subgroups with different risk profiles, as reflected in their volatilities. Bayesian model comparison criteria favor the model with component specific regression coefficients for volatilities. The subgroup with lower volatility exhibits a larger variance and, hence, a greater level of heterogeneity.

*Keywords:* First hitting time model; Finite mixture model; Frailty; Bayesian estimation; Model comparison

---

\*Email address: [yuan.huang@yale.edu](mailto:yuan.huang@yale.edu); corresponding author

# 1 Introduction

Hypoglycemia represents a significant adverse effect in glucose management and is a focal point of diabetes clinical research (Fu et al., 2016; Ma et al., 2021). Patients with diabetes display diverse reactions or responses to their treatment regimens. For instance, in the 24-week DURABLE trial (Buse et al., 2009), experiences of hypoglycemia among patients varied widely: some faced more than 100 episodes, underscoring it as a potential adverse effect of glucose management, while others seldom experienced any. This marked variability in hypoglycemia risk highlights the presence of substantial unobserved heterogeneity within the patient population. Tailoring treatment plans to specific patient subgroups, rather than adopting a “one size fits all” approach, may offer more effective diabetes management strategies (Qu et al., 2022; Jiang et al., 2018).

In practical healthcare settings, hypoglycemia episodes are typically self-reported by patients, facilitated by the occurrence of distinct symptoms such as headaches, hunger, and rapid heartbeat that serve as clear indicators of critically low glucose levels (Cryer et al., 2003). The pronounced and prompt manifestation of these symptoms enables patients to identify and report hypoglycemia episodes, thereby supporting accurate and timely documentation of such events. On the other hand, hyperglycemia, characterized by elevated glucose levels, often lacks overt symptoms that are immediately recognizable to the patient, making its detection more complex and generally requiring clinical intervention through blood tests. Given these significant differences in the observability of symptoms between hypoglycemia and hyperglycemia, the DURABLE trial (Buse et al., 2009) specifically opted to gather data only on hypoglycemic events that could be reliably reported by patients.

The First Hitting Time (FHT) model (Whitmore, 1986; Lee and Whitmore, 2003; Aalen and Gjessing, 2001) offers a refined approach for modeling time-to-event data, particularly in medical scenarios where it is crucial to predict the timing of specific health events. This model conceptualizes events as the moment an underlying stochastic process, such as a patient’s evolving health condition, crosses a predefined threshold (Lee, 2019), which could

signify a critical health event like hypoglycemia. Threshold regression, which incorporates covariate effects into model parameters such as the volatility of a Wiener process, enhances the precision of the FHT model. By accounting for individual patient characteristics, it provides more accurate predictions of event times (Lee and Whitmore, 2006). The challenge of modeling unobserved heterogeneity is commonly addressed by incorporating random effects (Pennell et al., 2010; Malefaki et al., 2015; Economou et al., 2015) or mixture components (Whitmore and Su, 2007; Lee et al., 2008; Race and Pennell, 2021) through their respective modifications of the FHT model. As this work focuses on mixture threshold regression models, a comprehensive review of recurrent event modeling is beyond the scope of this paper; we refer interested readers to recent reviews for the topics (Cook and Lawless, 2007; Charles-Nelson et al., 2019).

Applying the FHT model to hypoglycemia involves specific challenges, particularly in accurately modeling the dynamics of blood glucose levels. Blood glucose fluctuations can naturally be represented by Brownian motion, reflecting the unpredictable changes influenced by insulin administration, dietary intake, and physical activity. This stochastic representation is key to understanding the risk and occurrence of hypoglycemic events, marked by glucose levels crossing a lower boundary indicative of critically low glucose levels. Earlier studies have adapted the FHT model for recurrent hypoglycemic events, employing sequences of Brownian motions with reflective barriers to account for physiological expectations that glucose levels will eventually decrease, often due to the action of glucose-lowering medications (Xie et al., 2025). However, the detection of a bi-modal distribution in the fitted subject-level random effects suggests the existence of significant heterogeneity in the patient population, underscoring the need for a more nuanced modeling approach.

To address this gap, we propose a finite mixture FHT model tailored to the reflected Brownian motion process to capture the unobserved heterogeneity among patients with recurrent hypoglycemic events. By incorporating subject-level covariates and random effects, the model differentiates patient risk profiles, enabling a more individualized analysis of hy-

poglycemia risk. This approach offers insights into the impacts of different heterogeneity on recurrent hypoglycemic events, marking a significant contribution to personalized diabetes care. Model parameters are estimated in a Bayesian framework with Markov chain Monte Carlo (MCMC). Different distributional specifications of the random effects are evaluated via model selection criteria. Through extensive simulation studies and application to a motivating data, our research broadens the application of the FHT model, providing novel opportunities for a more comprehensive understanding and improved management of diabetes. The proposed methodology extends the non-mixture recurrent event model based on the FHT of reflected Brownian motion developed in [Xie et al. \(2025\)](#) to a finite mixture model for capturing additional unobserved heterogeneity in recurrent hypoglycemic events.

The structure of the remainder of this paper is as follows. Section 2 introduces the analysis data based on the DURABLE study and discuss existing studies. In Section 3, a mixture FHT model of reflected Brownian motion is proposed and Bayesian parameter estimation and model selection methods are presented. An application of the methods is given in Section 4. Simulation studies that validate the Bayesian inferences are reported in Section 5. A discussion is provided in Section 6.

## 2 Data and Challenge

The DURABLE trial ([Buse et al., 2009](#)) compared the efficacy of two starter insulin regimens, insulin lispro mix 75/25 versus insulin glargine, in achieving glycemic control for type 2 diabetes patients. The study enrolled 2187 patients from 11 countries. During the trial, the timing (in days) of hypoglycemic events was recorded for each patient over their follow-up period, which had a median duration of 168 days. We analyzed a synthetic dataset derived from the original DURABLE trial, in which covariates were lightly perturbed while the original event gap times were preserved. This ensures privacy protection while retaining the key features that motivate the current study. The dataset includes baseline covariates

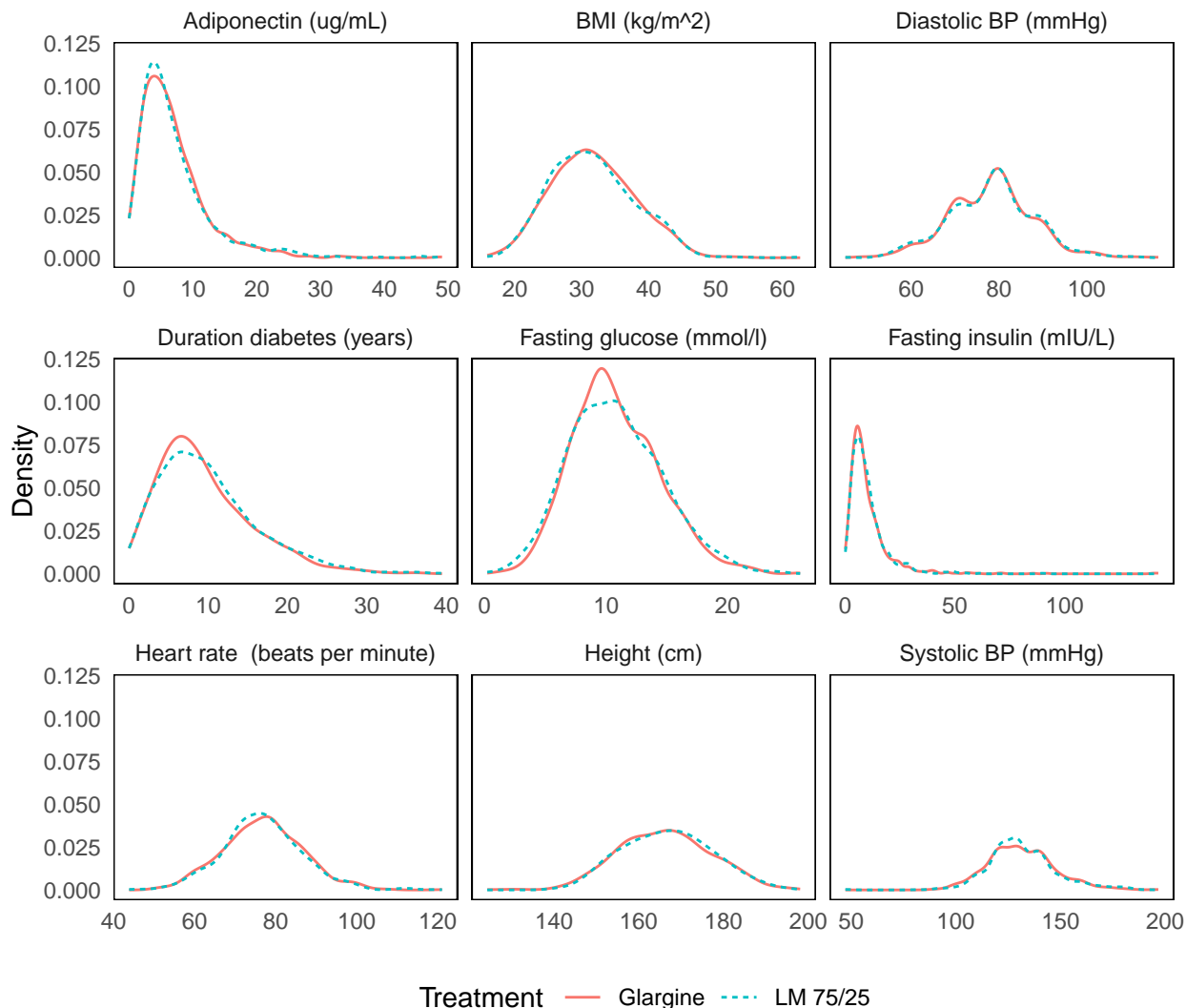


Figure 1: Distributions for continuous covariates by insulin starter regimens.

for each patient, such as fasting insulin, adiponectin, fasting blood glucose, height, body mass index (BMI), heart rate, diastolic and systolic blood pressure, and duration of diabetes, which are crucial for identifying risk factors associated with hypoglycemic events. Figure 1 displays the distributions of continuous baseline covariates by treatment group, showing little difference between the two regimens at baseline. Descriptive statistics of the continuous covariates are presented in Section 1 of Supplementary Materials. The dataset also includes two categorical variables: one indicating the type of oral antihyperglycemic drugs used—categorized as thiazolidinedione, sulfonylurea, or both—and another denoting

the assigned starter insulin regimen, comparing twice-daily lispro mix 75/25 (LM75/25; 75% lispro protamine suspension and 25% lispro) with once-daily insulin glargine.

The dataset for our study contained  $n = 1943$  patients after excluding the subjects with missing value or data points outside the reference range. To prepare for the analysis, we log-transformed adiponectin level and fasting insulin level, which have extremely high values, and standardized all the continuous covariates. Among these patients, 1207 (62%) received sulfonylurea alone, 166 (9%) received thiazolidinedione alone, and 570 (29%) received both oral antihyperglycemic drugs. For ease of discussion, we set the group receiving both drugs as the reference group. Two dummy variables, “sulf-Only” (equal to 1 if only sulfonylurea was received) and “tzd-only” (equal to 1 if only thiazolidinedione was received), were created. An indicator variable, denoted as “LM”, is used to signify the type of insulin starter regimen, with a value of 1 assigned to the 959 (49%) patients receiving LM 75/25 and 0 to the 984 (51%) patients administered glargine.

The daily hypoglycemic event rates exhibited substantial variability, ranging from 0 to 0.77, with an average rate of 0.07. There were 608 patients experienced more than one hypoglycemic event within a single day. This variability highlights the potential need for our proposed model to account for the diverse risk profiles within the diabetic patient cohort.

We briefly review the modeling framework proposed in [Xie et al. \(2025\)](#), which serves as the foundation for the mixture extension developed in this paper. [Xie et al. \(2025\)](#) modeled hypoglycemic events by the FHT of a reflected Brownian motion. This approach conceptualizes the recurrent hypoglycemic events as a sequence of Brownian motion reflected from above, each hitting a lower boundary, followed by a reset of the process at a predetermined level. The upper reflection barrier of the Brownian motion allows bypassing the need for capturing hyperglycemic event times, which are often unreliable or unobservable in self-reported datasets. The gap times between the successive events of the same patient are assumed to be independent conditional on a subject-specific frailty, which follow a FHT distribution of the associated reflected Brownian motion. The distribution and density functions investi-

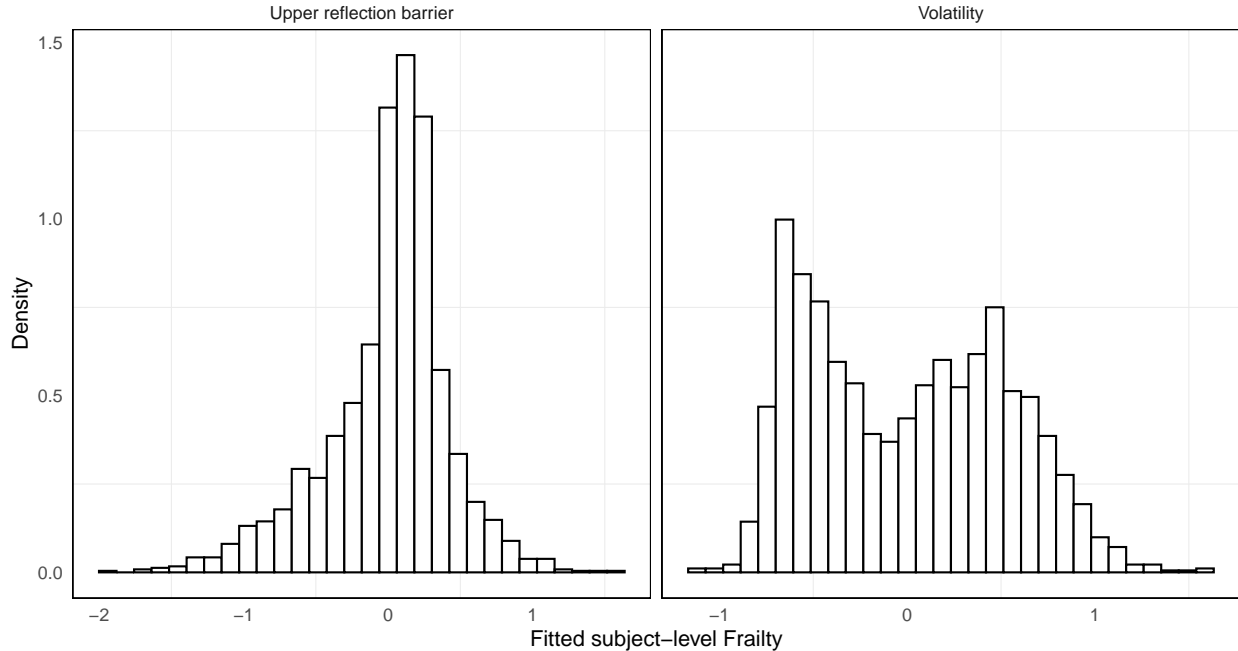


Figure 2: The histogram of the posterior mean of the fitted subject-level frailty in upper reflecting barrier (left) and volatility (right)

gated by [Hu et al. \(2012\)](#) are presented in Appendix A for completeness. Random number generation from the distribution can be developed with a rejection sampling algorithm. In the modeling framework, the subject-level frailty and covariates were linked to the volatility and the upper reflecting barrier of the Brownian motion.

Incorporating subject-level frailty into the model is crucial for capturing heterogeneity among patients. The estimated frailty variance in the volatility model was 0.535 with 95% credible interval (0.450, 0.620), which significantly deviates from zero ([Xie et al., 2025](#)). This result reflects the heterogeneity in hypoglycemic event rates among patients. Further scrutiny of the fitted subject-level frailty reveals a bi-modal pattern in the histogram as shown in Figure 2. This pattern suggests unobserved heterogeneity beyond covariates and subject-level frailty, which might be captured by a mixture model. Mixture models are commonly used to handle unobserved heterogeneity among patients from different subpopulations. Covariate coefficients can be constructed as component-specific, which allows for diverse effects of the treatments on patients from different groups. Furthermore, positing that frailties for patients

from different subgroups adhere to different distributions emerges as a reasonable and logical step forward. Given these considerations, we advance the framework of Xie et al. (2025) to a finite mixture FHT model tailored to the analysis of recurrent hypoglycemic events, thereby aiming to more accurately capture the intricate heterogeneity within the patient data.

### 3 Methods

This section introduces the finite mixture FHT model, presents its Bayesian formulation, and outlines the associated reduced models and model selection criteria.

#### 3.1 A FHT Mixture Model for Recurrent Events

We propose a mixture FHT frailty model with  $K$  components to further capture the heterogeneity among subgroups. To address the specific motivating problem presented in Section 2, we consider the volatility  $\sigma$  of the Brownian motion to be component-specific, with  $K = 2$ . Suppose that subject  $i$  belongs to the  $k$ th component of the mixture model with weight  $\rho_k$ , where  $\sum_{k=1}^2 \rho_k = 1$ . Denoting  $\boldsymbol{\sigma}_i = (\sigma_{i1}, \sigma_{i2})$ ,  $\boldsymbol{\rho} = (\rho_1, \rho_2)$ , the  $j$ th gap time  $t_{ij}$  of subject  $i$  is assumed to be drawn from the mixture density

$$p(t_{ij}|\boldsymbol{\rho}, x_0, \nu, \kappa_i, \boldsymbol{\sigma}_i) = \sum_{k=1}^2 \rho_k f(t_{ij}|x_0, \nu, \kappa_i, \sigma_{ik}),$$

where  $f(\cdot)$  denotes the FHT density function defined in (A.1), and  $x_0$  and  $\nu$  represent the preset starting point and the lower boundary of the Brownian motion, respectively,  $\kappa_i$  is the upper reflection barrier of the Brownian motion for subject  $i$ , and  $\sigma_{ik}$  represents the volatility of the Brownian motion for subject  $i$  in the  $k$ th component. Typically, a smaller upper reflection barrier or a larger volatility is associated with an increased risk of hypoglycemic events.

Subject-level covariate and frailty are incorporated into the upper reflection barrier  $\kappa_i$  and

the volatility  $\sigma_{ik}$  with logarithmic link. Let  $\mathbf{X}_i = (1, X_{i1}, \dots, X_{ip})^\top$  be a time-independent covariate vector of subject  $i$ . The models for  $\sigma_{ik}$  and  $\kappa_i$  are given by

$$\log(\sigma_{ik}) = \mathbf{X}_i^\top \boldsymbol{\beta}_k + Z_{1ik}, \quad \text{and} \quad \log(\kappa_i - x_0) = \mathbf{X}_i^\top \boldsymbol{\alpha} + Z_{2i}, \quad (3.1)$$

where  $\boldsymbol{\alpha} = (\alpha_0, \alpha_1, \dots, \alpha_p)^\top$  is the regression coefficient vector in upper reflection barrier;  $\boldsymbol{\beta}_k = (\beta_{k0}, \beta_{k1}, \dots, \beta_{kp})^\top$ ,  $k = 1, 2$ , is the component-specific regression coefficient vector for the volatility.  $Z_{1ik}$  and  $Z_{2i}$  are the independent random effects following normal distribution with mean 0 and variance  $\theta_{1k}$  and  $\theta_2$ , respectively. Only the volatility is allowed to have component-specific regression coefficients, as extending this flexibility to the upper reflection barrier would substantially increase model complexity and hinder MCMC convergence.

### 3.2 Likelihood, prior, and posterior

Assume that hypoglycemic event times are observed from  $n$  patients during their follow-up periods. For subject  $i$ ,  $i = 1, \dots, n$ , let  $T_{ij}$ ,  $j = 1, \dots, n_i$ , denote the observed time of the  $j$ th observation, where the final observation is censored. The gap times between two successive events are denoted as  $t_{ij} = T_{ij} - T_{i(j-1)}$ , where  $T_{i0} = 0$ . For notation generality, define the event indicator  $\delta_{ij} = 1$  for  $j \neq n_i$ , indicating an event observation, and 0 otherwise indicating a censored observation. That is, the only censored observations are the final one for each subject. For subject  $i$ , the observed data is given by  $\mathbf{D}_i = \{\mathbf{X}_i, \mathbf{t}_i, \boldsymbol{\delta}_i\}$ , where  $\mathbf{t}_i = (t_{i1}, \dots, t_{in_i})^\top$  and  $\boldsymbol{\delta}_i = (\delta_{i1}, \dots, \delta_{in_i})^\top$ . The observed data for all the subjects are denoted by  $\mathbf{D} = (\mathbf{D}_1, \dots, \mathbf{D}_n)$ .

Given the covariate vector  $\mathbf{X}_i$ , the latent membership  $m_i$ , and subject-level frailties  $\mathbf{z}_i = (z_{1im_i}, z_{2i})$ , the gap times of subject  $i$  are assumed to be conditionally independent. Let  $\boldsymbol{\Omega} = (\boldsymbol{\alpha}^\top, \boldsymbol{\beta}_1^\top, \boldsymbol{\beta}_2^\top)^\top$ , the conditional likelihood contribution of subject  $i$  given the frailties

and the membership can be written as

$$L_i(\boldsymbol{\Omega}|\mathbf{D}_i, \mathbf{z}_i, m_i) = \prod_{j=1}^{n_i} [f(t_{ij}|x_0, \nu, \kappa_i, \sigma_{im_i})]^{\delta_{ij}} [1 - F(t_{ij}|x_0, \nu, \kappa_i, \sigma_{im_i})]^{(1-\delta_{ij})},$$

where the density  $f$  and distribution  $F$  functions are given in (A.1) and (A.2), respectively, and  $\sigma_{im_i}$  and  $\kappa_i$  are defined in (3.1).

The recorded event times are usually discrete in the unit of days. In this case, the gap time  $t_{ij}$ 's are handled as interval-censored. The likelihood contribution for subject  $i$  can then be rewritten as

$$L_i(\boldsymbol{\Omega}|\mathbf{D}_i, \mathbf{z}_i, m_i) = \prod_{j=1}^{n_i} [F^*(t_{ij}|x_0, \nu, \kappa_i, \sigma_{im_i})]^{\delta_{ij}} \times \left[ 1 - F\left(t_{ij} + \frac{1}{2} \middle| x_0, \nu, \kappa_i, \sigma_{im_i}\right) \right]^{(1-\delta_{ij})}, \quad (3.2)$$

where

$$F^*(t_{ij}|x_0, \nu, \kappa_i, \sigma_{im_i}) = F\left(t_{ij} + \frac{1}{2} \middle| x_0, \nu, \kappa_i, \sigma_{im_i}\right) - F\left(t_{ij} - \frac{1}{2} \middle| x_0, \nu, \kappa_i, \sigma_{im_i}\right).$$

Under the Bayesian framework, prior distributions for the model parameters need to be specified. For regression coefficients  $\boldsymbol{\alpha}$  and  $\boldsymbol{\beta}_k$ , we assign noninformative normal priors with zero mean and large variance. Inverse-Gamma priors are specified for the normal variances of the frailties  $\theta_{1k}$  and  $\theta_2$ . Dirichlet distribution is assigned as prior for mixture weights. The priors are summarized as follows:

$$\begin{aligned} \boldsymbol{\rho} &= (\rho_1, \rho_2) \sim \text{Dirichlet}(\boldsymbol{\xi}), \\ \alpha_l &\sim N(0, \sigma_\alpha^2), \quad l = 0, \dots, p, \\ \beta_{kl} &\sim N(0, \sigma_\beta^2), \quad l = 0, \dots, p, \quad k = 1, 2 \\ \theta_{1k} &\sim \text{Inv-Gamma}(a, b), \quad k = 1, 2, \\ \theta_2 &\sim \text{Inv-Gamma}(a, b), \end{aligned} \quad (3.3)$$

where  $\text{Dirichlet}(\boldsymbol{\xi})$  is the Dirichlet distribution with concentration parameters vector  $\boldsymbol{\xi}$ ,  $N(0, \sigma_\alpha^2)$  and  $N(0, \sigma_\beta^2)$  are the normal distributions with mean zero and variance  $\sigma_\alpha^2 > 0$  and  $\sigma_\beta^2 > 0$ , respectively, and  $\text{Inv-Gamma}(a, b)$  is the inverse gamma distribution with shape  $a > 0$  and scale  $b > 0$ . In our data analysis and simulation studies, the hyper-parameters were set to be  $\sigma_\alpha^2 = \sigma_\beta^2 = 10^2$ ,  $a = b = 1$ , and  $\boldsymbol{\xi} = (1, 1)$ .

To derive the joint posterior distribution, let  $\boldsymbol{\Gamma} = (\boldsymbol{\Omega}, \boldsymbol{\rho}, \theta_{11}, \theta_{12}, \theta_2)^\top$  denote the collection of model parameters. With  $\mathbf{z} = (\mathbf{z}_1, \dots, \mathbf{z}_n)^\top$  and  $\mathbf{m} = (m_1, \dots, m_n)^\top$ , the joint posterior density is obtained by combining the likelihood function and the prior distributions,

$$\begin{aligned} \pi(\boldsymbol{\Gamma}, \mathbf{z}, \mathbf{m} \mid \mathbf{D}) \propto & \left[ \prod_{i=1}^n L_i(\boldsymbol{\Omega} \mid \mathbf{D}_i, \mathbf{z}_i, m_i) g(\mathbf{z}_i \mid \theta_{1m_i}, \theta_2, m_i) g(m_i \mid \boldsymbol{\rho}) \right] \\ & \times q(\boldsymbol{\alpha}) q(\boldsymbol{\beta}_1) q(\boldsymbol{\beta}_2) q(\boldsymbol{\rho}) q(\theta_{11}) q(\theta_{12}) q(\theta_2), \end{aligned}$$

where  $L_i(\boldsymbol{\Omega} \mid \mathbf{D}_i, \mathbf{z}_i, m_i)$  is the conditional likelihood function for subject  $i$  given in (3.2),  $g(\mathbf{z}_i \mid \theta_{1m_i}, \theta_2, m_i)$  is the bivariate independent normal density of the frailties of subject  $i$  given membership  $m_i$ ,  $g(m_i \mid \boldsymbol{\rho})$  is the probability mass function of categorical distribution with probability vector  $\boldsymbol{\rho}$ , and  $q(\cdot)$  denotes a generic density function of its argument and all the  $q(\cdot)$ 's are priors given in (3.3). Since all the priors are proper, the posterior is proper.

We employ MCMC to make inference about the parameters. Since the FHT density of the reflected Brownian motion does not have any standard form, we apply the Metropolis-Hastings random walk algorithm to sample from the full conditional distributions of all the parameters. The implementation could be done through a generic R package NIMBLE (de Valpine et al., 2017). The model implementation details are presented in Section 5 of the Supplementary Materials, which also briefly discusses how the label switching issue is handled by imposing ordering constraint on the parameters during MCMC using NIMBLE. This constraint-based approach avoids the need for post-processing relabeling algorithms, for which methods such as Stephens (2000) and implementations summarized in Papastamoulis (2016) are widely used. Due to the considerable number of unobserved frailties and

Table 1: Summary of candidate models. CS-C-FV: component-specific coefficients and frailty variances model; CS-I-FV: component-specific intercept and frailty variances model; CS-I: component-specific intercept model; CS-N: none component specific (single component frailty model)

Model	Volatility $\sigma_{ik}$	Constraint
CS-C-FV	$\log(\sigma_{ik}) = \mathbf{X}_i^\top \boldsymbol{\beta}_k + Z_{1ik}$ $Z_{1ik} \sim N(0, \theta_{1k})$	
CS-I-FV	$\log(\sigma_{ik}) = \beta_{k0} + \sum_{l=1}^p X_{il}\beta_l + Z_{1ik}$ $Z_{1ik} \sim N(0, \theta_{1k})$	$\beta_l = \beta_{1l} = \beta_{2l}$ for $l = 1, \dots, p$
CS-I	$\log(\sigma_{ik}) = \beta_{k0} + \sum_{l=1}^p X_{il}\beta_l + Z_{1ik}$ $Z_{1ik} \sim N(0, \theta_{11})$	$\beta_l = \beta_{1l} = \beta_{2l}$ for $l = 1, \dots, p$ , and $\theta_{11} = \theta_{12}$
CS-N	$\log(\sigma_i) = \beta_0 + \sum_{l=1}^p X_{il}\beta_l + Z_{1i}$ $Z_{1i} \sim N(0, \theta_1)$	Only one component

membership, the resulting chains exhibit strongly auto-correlation. A sufficient number of posterior draws can be retained after thinning the long chains, which also helps reduce the computational burden associated with calculating the model comparison criteria described in a later section.

### 3.3 Reduced models and model selection criteria

Given the setup in (3.1) as the full model, several reduced models are proposed. Model 2 is a reduced model of the full model, imposing the restriction that both components share identical regression coefficients, i.e.,  $\beta_{1l} = \beta_{2l}$  for  $l = 1, \dots, p$ . This assumption suggests that covariates have the same impact across different population subgroups. Model 3 further simplifies Model 2 by constraining the frailty variances of the two components to be identical, denoted as  $\theta_{11} = \theta_{12}$ . This assumption indicates that the frailties of both components are expected to be from the same distribution. For ease of reference, we classify the models based on whether the covariate coefficients or frailty variances are component-specific (CS). Accordingly, we label the full and the two reduced models as the CS-C-FV (component-specific coefficients and frailty variances) model, the CS-I-FV (component-specific intercept

and frailty variances) model, and the CS-I (component-specific intercept) model, respectively. The independent-frailty model proposed by Xie et al. (2025) includes only single component is referred as CS-N (none component specific) model here. A comparative summary of these models is presented in Table 1.

Two model comparison criteria, deviance information criterion (DIC) (Spiegelhalter et al., 2002) and logarithm of the pseudo-marginal likelihood (LPML) (Geisser and Eddy, 1979; Gelfand and Dey, 1994) are considered to conduct model selection. For a candidate model, define deviance

$$\text{Dev}(\mathbf{\Gamma}) = -2 \sum_{i=1}^n \log L_{i,obs}(\mathbf{\Gamma}|\mathbf{D}_i),$$

where  $L_{i,obs}(\mathbf{\Gamma}|\mathbf{D}_i)$  is the contribution to the observed likelihood from subject  $i$ . The DIC is then defined as

$$\text{DIC} = \text{Dev}(\bar{\mathbf{\Gamma}}) + 2p_D,$$

where  $p_D = \overline{\text{Dev}}(\mathbf{\Gamma}) - \text{Dev}(\bar{\mathbf{\Gamma}})$  is the effective number of model parameters, and  $\bar{\mathbf{\Gamma}}$  and  $\overline{\text{Dev}}(\mathbf{\Gamma})$  are the posterior means of  $\mathbf{\Gamma}$  and  $\text{Dev}(\mathbf{\Gamma})$ , respectively. A lower value of DIC means a better model.

As there is no closed form for the observed data likelihood which integrates out all the latent variables, Monte Carlo approximation is used to approximate the integral. The observed data likelihood of subject  $i$  has the form

$$L_{i,obs}(\mathbf{\Gamma}|\mathbf{D}_i) = \sum_{k=1}^2 g(m_i = k|\boldsymbol{\rho}) \int L_i(\boldsymbol{\Omega}|\mathbf{D}_i, \mathbf{z}_i, m_i = k) g(\mathbf{z}_i|\theta_{1m_i}, \theta_2, m_i = k) d\mathbf{z}_i,$$

where  $\mathbf{\Gamma}$  is the set of model parameters and  $L_i(\boldsymbol{\Omega}|\mathbf{D}_i, \mathbf{z}_i, m_i)$  is given in (3.2). The random effects  $\mathbf{z}_i$  are continuous, and the corresponding integral is approximated using Monte Carlo integration. In contrast, the latent membership  $m_i$  is a discrete random variable taking values in  $\{1, 2\}$ , and integration with respect to  $m_i$  is performed by summation over its

possible values. Then the observed data likelihood for subject  $i$  can be derived by

$$L_{i,obs}(\mathbf{\Gamma}|\mathbf{D}_i) \approx \sum_{k=1}^2 g(m_i = k|\boldsymbol{\rho}) \left[ \frac{1}{S} \sum_{s=1}^S L_i(\boldsymbol{\Omega}|\mathbf{D}_i, \mathbf{z}_i^{(s)}, m_i = k) \right], \quad (3.4)$$

where  $\mathbf{z}_i^{(1)}, \dots, \mathbf{z}_i^{(S)}$  are Monte Carlo samples that each can be generated independently from a bivariate normal distributions  $N(\mathbf{0}, \boldsymbol{\Sigma})$ , where the covariance matrix  $\boldsymbol{\Sigma} = \text{diag}(\theta_{1m_i}, \theta_2)$  conditional on  $m_i$ , and  $S$  is the Monte Carlo sample size.

LPML is calculated based on conditional predictive ordinate (CPO). Let  $D_{-i} = \{(\mathbf{t}_j, \boldsymbol{\delta}_j, X_j) : j = 1, \dots, n; j \neq i\}$ , denote the observed data without the  $i$ th subject. The CPO for the  $i$ th subject is the leave-one-out predictive likelihood

$$\text{CPO}_i = \int L_{i,obs}(\mathbf{\Gamma}|\mathbf{D}_i)q(\mathbf{\Gamma}|D_{-i})d\mathbf{\Gamma},$$

where  $q(\mathbf{\Gamma}|D_{-i})$  is the marginal posterior distribution of  $\mathbf{\Gamma}$  with the  $i$ th subject deleted. The Monte Carlo estimate of  $\text{CPO}_i$  (Dey et al., 1997) is given by

$$\widehat{\text{CPO}}_i = \left[ \frac{1}{U} \sum_{u=1}^U \frac{1}{L_{i,obs}(\mathbf{\Gamma}^{(u)}|\mathbf{D}_i)} \right]^{-1}, \quad (3.5)$$

where  $\mathbf{\Gamma}^{(u)} = (\boldsymbol{\alpha}^{(u)}, \boldsymbol{\beta}_1^{(u)}, \boldsymbol{\beta}_2^{(u)}, \boldsymbol{\rho}^{(u)}, \theta_{11}^{(u)}, \theta_{12}^{(u)}, \theta_2^{(u)})$ , for  $u = 1, \dots, U$ , denotes the  $u$ th MCMC draw from the posterior distribution, and  $U$  is the total number of posterior draws. Each term  $L_{i,obs}$  in (3.5) can be approximated the same way as in (3.4). Then LPML can be calculated by

$$\widehat{\text{LPML}} = \sum_{i=1}^n \log(\widehat{\text{CPO}}_i).$$

Models with higher LPML are preferred.

The calculation of model comparison criteria is based on the observed data likelihood, which requires integrating all the random effects and latent memberships out. This process is computationally intensive. To reduce the computational burden, we used a relatively small

Table 2: Model comparison for the four models fitted to the motivating data. A lower value of DIC (deviance information criterion) and a higher value of LPML (logarithm of the pseudo-marginal likelihood) indicate a better model.

	CS-C-FV	CS-I-FV	CS-I	CS-N
DIC	130843.3	130871.8	130947.3	131344.0
LPML	-65444.2	-65449.2	-65498.5	-65676.7

number of posterior samples to calculate the model comparison criteria in our simulation study.

## 4 Results

Three proposed models were applied to analyze the motivating data. The priors for all the parameters were specified as shown in Section 3.2. The lower boundary  $\nu$  was set to 3.9 mmol/l (70 mg/dl), which is the clinical standard for hypoglycemic events (Seaquist et al., 2013). The starting point  $x_0$  of the Brownian motion after each hypoglycemic event was set to be 10, which is the rounded integer of the median of the baseline fasting glucose level of all patients. For each model, an MCMC was run for 150,000 iterations and thinned by 10 after discarding the first 30,000 iterations as burn-in. Sensitivity analysis about the alternative starting values of some parameters are presented in Supplementary Materials Section 4.2. The convergence of the MCMC chains was monitored by traceplots, which are shown in the Section 2 of the Supplementary Materials. The results of DIC and LPML for the three models are presented in Table 2, alongside the results for the independent-frailty model (referred as CS-N in this study) as reported by Xie et al. (2025). Both DIC and LPML favor the full model, CS-C-FV model, which suggests that component-specific regression coefficients and frailty variances are crucial for capturing differing covariate effects and unobserved heterogeneity, respectively between the two subgroups.

The posterior density for the regression coefficients related to volatility of the CS-C-FV

Table 3: Estimated parameters of the CS-C-FV model. BMI, body mass index; BP, blood pressure; SD, standard deviation; CI, 95% HPD credible interval or 95% confident interval.

Covariates	Volatility						Upper reflection barrier		
	Group 1			Group 2			Mean	SD	95% CI
	Mean	SD	95% CI	Mean	SD	95% CI			
Intercept	-0.171	0.130	[-0.411, 0.072]	1.410	0.027	<b>[1.357, 1.458]</b>	2.839	0.062	<b>[2.715, 2.955]</b>
Fasting glucose	-0.139	0.051	[-0.24, -0.04]	-0.016	0.013	[-0.041, 0.009]	0.11	0.031	<b>[0.051, 0.17]</b>
Adiponectin	0.134	0.066	<b>[0.016, 0.267]</b>	0.019	0.012	[-0.004, 0.043]	0.034	0.03	[-0.026, 0.09]
Fasting insulin	-0.272	0.056	[-0.381, -0.159]	-0.036	0.014	<b>[-0.062, -0.008]</b>	0.164	0.032	<b>[0.096, 0.222]</b>
Height	0.067	0.050	[-0.024, 0.174]	-0.049	0.013	<b>[-0.072, -0.023]</b>	0.019	0.03	[-0.035, 0.081]
BMI	-0.092	0.061	[-0.209, 0.024]	-0.046	0.012	<b>[-0.069, -0.02]</b>	-0.11	0.033	<b>[-0.17, -0.043]</b>
Diastolic BP	-0.064	0.062	[-0.188, 0.049]	-0.023	0.015	[-0.052, 0.005]	0.061	0.034	[-0.005, 0.128]
Systolic BP	0.053	0.062	[-0.068, 0.176]	0.007	0.013	[-0.019, 0.032]	-0.023	0.031	[-0.08, 0.042]
Heart rate	0.082	0.062	[-0.03, 0.204]	0.000	0.012	[-0.022, 0.023]	0.05	0.028	[-0.002, 0.105]
Duration diabetes	0.190	0.047	<b>[0.092, 0.274]</b>	0.020	0.011	[-0.002, 0.044]	-0.043	0.027	[-0.091, 0.011]
LM	0.177	0.109	[-0.021, 0.385]	0.092	0.023	<b>[0.047, 0.137]</b>	-0.124	0.056	<b>[-0.24, -0.027]</b>
tzd-only	-0.445	0.200	<b>[-0.828, -0.073]</b>	-0.166	0.060	<b>[-0.282, -0.054]</b>	0.396	0.144	<b>[0.129, 0.682]</b>
sulf-only	0.058	0.120	[-0.187, 0.277]	-0.015	0.027	[-0.063, 0.044]	0.067	0.065	[-0.071, 0.188]
Frailty Std	0.773	0.051	<b>[0.674, 0.867]</b>	0.249	0.012	<b>[0.226, 0.274]</b>	0.699	0.027	<b>[0.647, 0.751]</b>
Mixture_Weight	0.440	0.023	<b>[0.399, 0.486]</b>	0.560	0.023	<b>[0.514, 0.601]</b>			

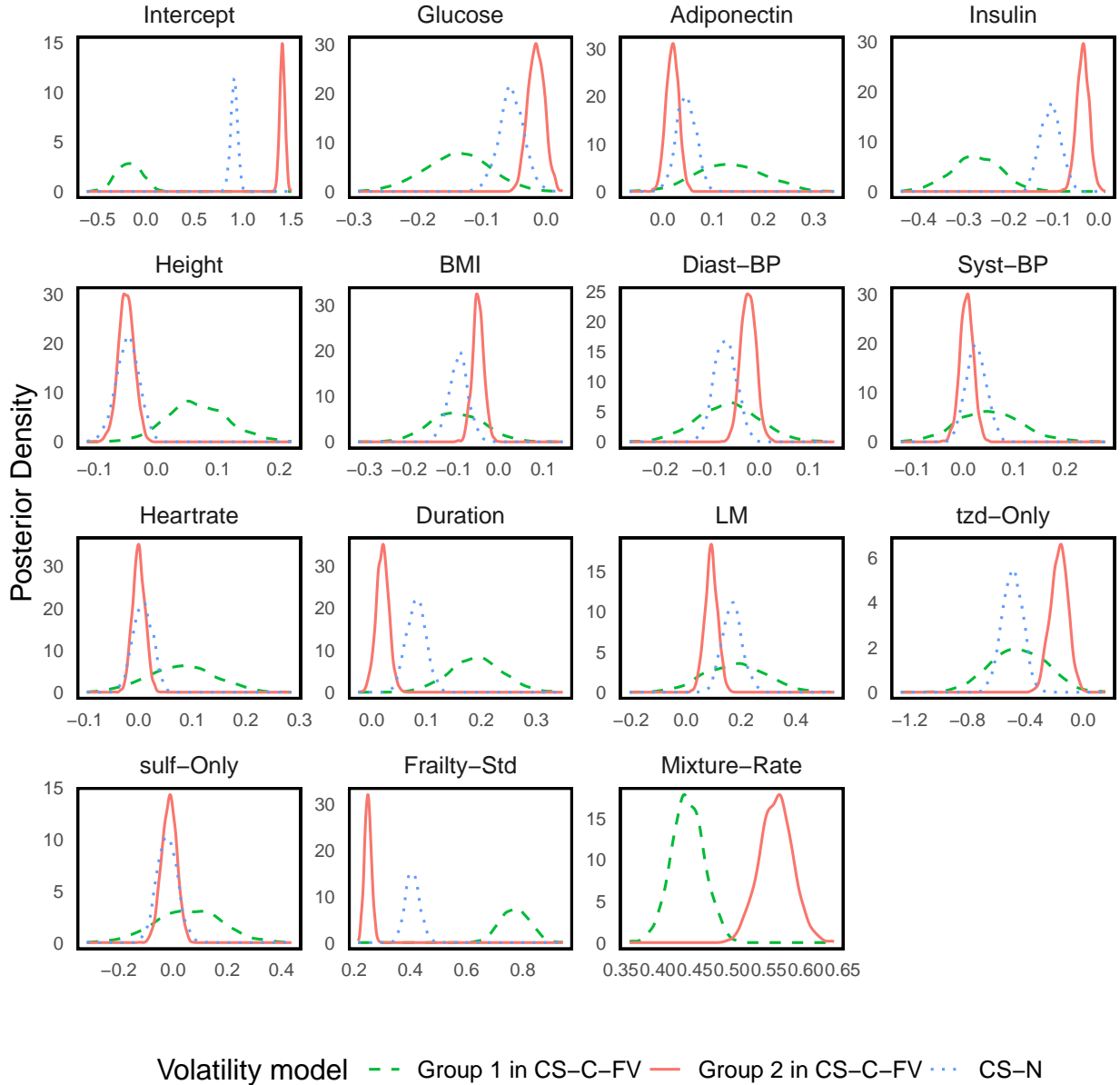


Figure 3: Posterior density of estimates in volatility model in CS-C-FV and CS-N model.

model and CS-N model are depicted in Figure 3. Additionally, the point estimate, standard error, and 95% highest posterior density (HPD) credible interval for all parameters of the CS-C-FV model are summarized in Table 3. From Table 3, we generally find that the covariate effects in the upper reflection barrier estimated by the CS-C-FV model are similar to those reported for the CS-N model by Xie et al. (2025). This similarity is anticipated since the mixture structure is considered solely in volatility. A more detailed examination of the

covariate effects in the volatility model, as depicted in Figure 3, reveals that the estimates from the CS-N model fall between the two groups from the CS-C-FV model. This indicates that the mixture structure offers richer and more informative characterization. Notably, all coefficients that are significant in the volatility model of the CS-N model remain significant in either group 1 or 2, with an exception of the baseline diastolic blood pressure. The comparison of the volatility intercept terms between the two groups indicates a significant difference. As mentioned in Section 3.1, in general, larger volatility is associated with an increased risk of hypoglycemic events. Hence, the significant difference in volatility intercept terms between the two groups justifies categorizing them as low risk (group 1) or high risk (group 2) for hypoglycemia, with a smaller intercept indicating lower risk and a larger intercept indicating higher risk. According to the estimates of the mixture weight, the proportions of the low-risk and high-risk groups are approximately 44% and 56%, respectively.

Among the low-risk group, patients with lower baseline fasting glucose, lower baseline fasting insulin, higher baseline adiponectin, longer duration of diabetes are associated with larger volatility so higher risk of hypoglycemic events. For the patients in the high-risk group, lower baseline fasting insulin, lower height, lower BMI are associated with a higher risk of hypoglycemia. High-risk patients who received LM75/25 appear to have higher volatility or a higher risk of hypoglycemia compared to those who received glargine. For oral antihyperglycemic drugs, regardless of the group, patients solely received thiazolidinedione appear to exhibit reduced volatility or a lower risk of hypoglycemia when compared to those received both thiazolidinedione and sulfonylurea. There is no significant difference in patients received solely with sulfonylureas compared to those receiving both oral antihyperglycemic medications.

For covariates significantly impacting both the low-risk and high-risk groups, baseline fasting insulin and **tzd-only**, we have included plots of the predictive distribution derived from the fitted parameters for the two groups in Figure 4. These illustrations demonstrate the influence of baseline insulin levels and the exclusive use of thiazolidinediones on the

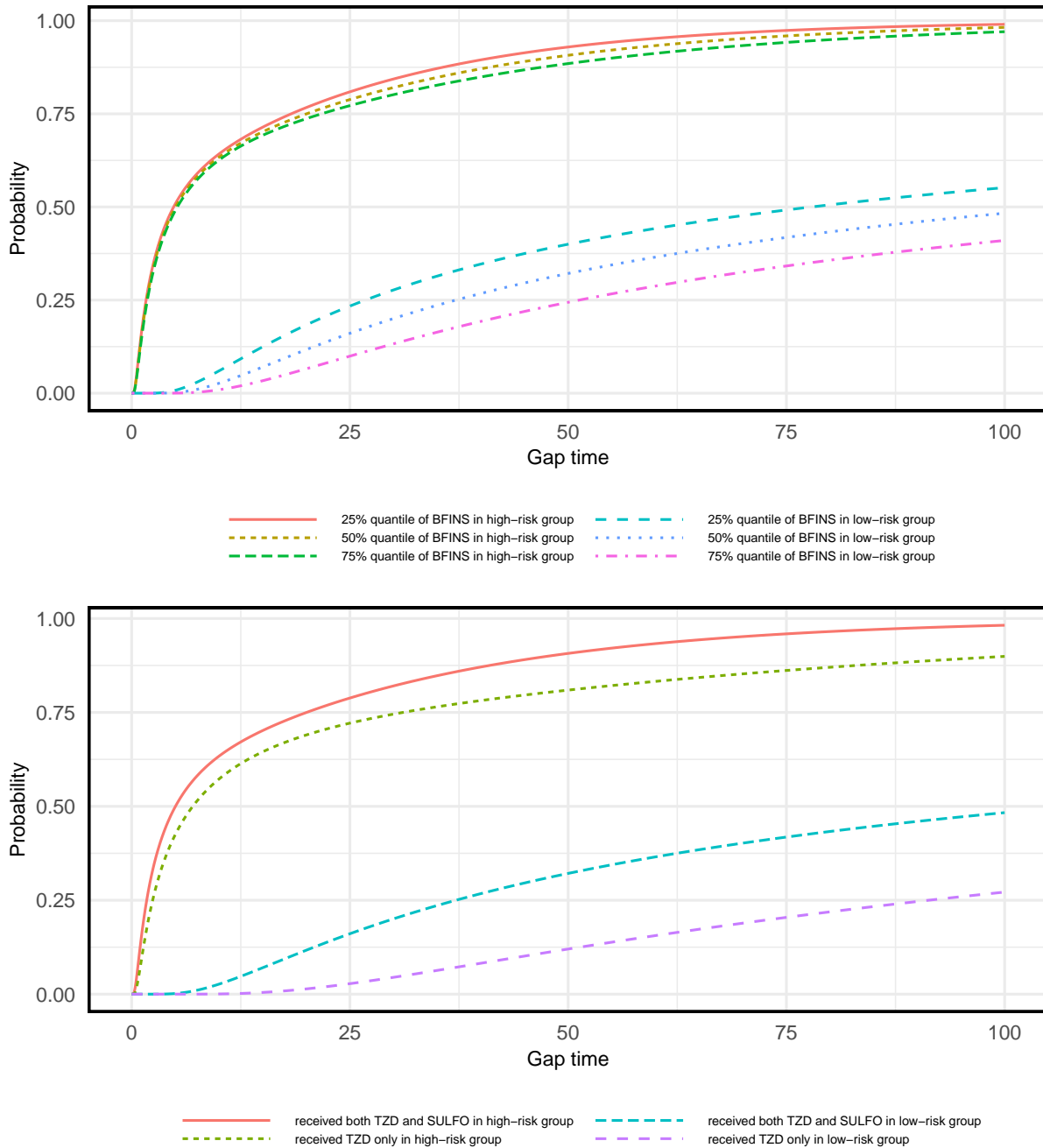


Figure 4: Predictive distribution functions were derived using the estimated parameters at different covariate levels by risk group. Three levels corresponding to the 25%, 50%, and 75% quantiles of baseline fasting insulin and two levels of *tzd-only* (0 and 1) were considered, shown in the top and bottom panels, respectively. BFINS: baseline fasting insulin; TZD: thiazolidinedione; SULFO: sulfonylurea.

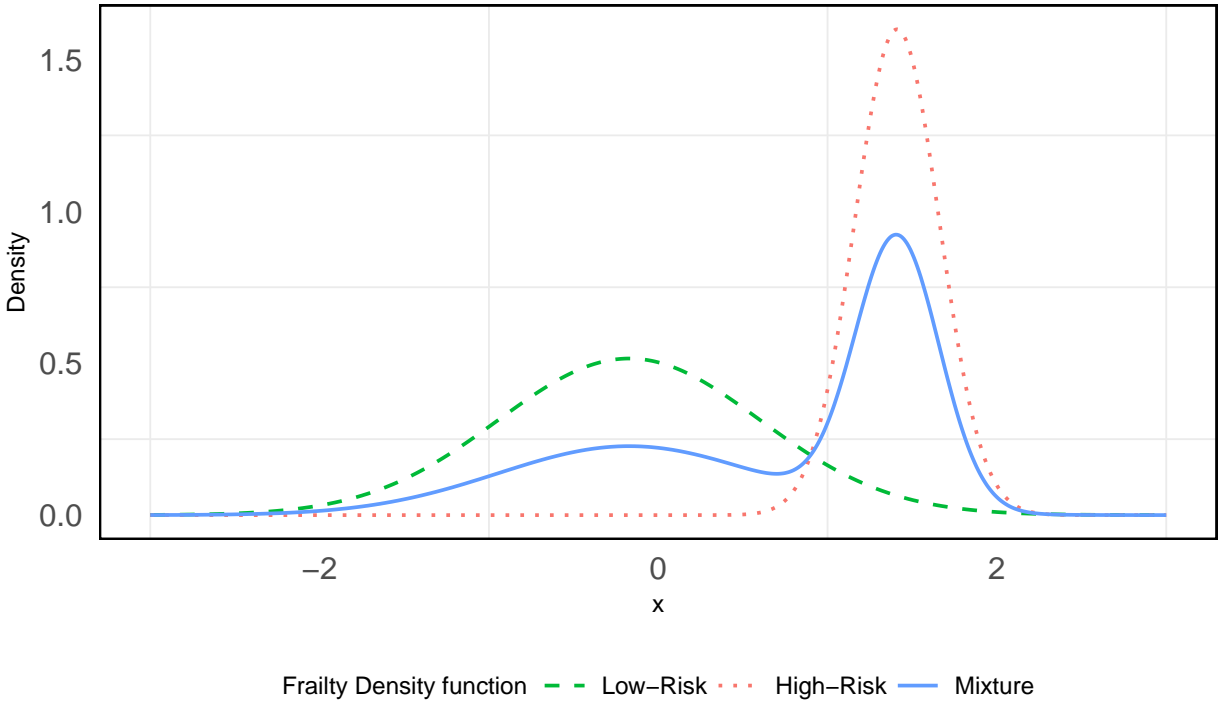


Figure 5: Frailty density functions for the low- and high-risk groups and the corresponding mixture frailty density function based on the estimated parameters.

distribution across the two groups. The figure indicates that when controlling other covariates at the same level, the median predictive gap time for patients within the high-risk group is substantially less compared to those in the low-risk group. This suggests a higher frequency of hypoglycemic events among high-risk patients. Additionally, the plot also highlights the distinct effects of various covariates on the two groups. As previously mentioned, for example, receiving both medications is associated with an increased risk of hypoglycemia when compared to only receiving thiazolidinedione. Upon further examination of the impact on different groups, it is observed that taking both medications significantly reduces the gap time for patients in the low-risk group more than in the high-risk group, indicating a markedly increased risk of hypoglycemia.

When we examine the variability in frailty across the two identified patient groups, a notable distinction emerges in frailty standard deviation. The frailty distributions for each group and the mixture frailty distribution are shown in Figure 5. Specifically, the high-

risk group is characterized by a relatively smaller standard deviation in frailty, suggesting a more homogenous reaction to hypoglycemic risk factors within this group. Conversely, the standard deviation is significantly larger in the low-risk group, pointing to a higher degree of between-subject variability. This greater variance within the low-risk group indicates that, despite being categorized as less susceptible to hypoglycemic events, there is a wide range of underlying susceptibilities and responses to treatment. This observation underscores the complexity of managing diabetes and highlights the importance of personalized treatment plans that consider the differences in patient responses, even within the same risk group.

In the upper reflection barrier model, patients with lower baseline fasting glucose, lower fasting insulin, higher BMI are associated lower upper reflection barrier or a higher risk of hypoglycemia. For the oral antihyperglycemic drugs, the patients only received thiazolidinedione appear to have a lower risk of hypoglycemia compared to those who received both two oral antihyperglycemic. Patients who received LM75/25 appear to have a lower reflection barrier or higher risk of hypoglycemia compared to those who received glargine. These results are similar to those reported in the earlier study.

## 5 Simulation

Simulation studies were conducted to assess the estimation procedure and model selection criteria. Two covariates were considered for each subject  $i$ :  $X_{i1}$ , baseline insulin level, and  $X_{i2}$ , baseline body mass index (BMI). To mimic the covariate structure in the motivating data, a bivariate gamma distribution with a normal copula was fitted using the R package `copula` (Hofert et al., 2018), and the two covariates were then generated from the fitted distribution.

Three mixture FHT models in Table 1 were used to generate recurrent event times with covariate vector  $\mathbf{X}_i = (1, X_{i1}, X_{i2})^\top$ . The true values of parameters in the full model were set with  $\boldsymbol{\alpha} = (2.9, 0.2, -0.1)^\top$ ,  $\boldsymbol{\beta}_1 = (-0.2, -0.3, -0.1)^\top$ ,  $\boldsymbol{\beta}_2 = (1.4, -0.05, -0.05)^\top$ , and

$\boldsymbol{\rho} = (0.4, 0.6)^\top$ . The frailties  $z_{1i1}$  and  $z_{1i2}$  in volatility for two groups were generated from the normal distribution with mean zero and variance  $\theta_{11} = 0.5$  and  $\theta_{12} = 0.1$ . The frailty  $z_{2i}$  in the upper reflection barrier was generated from the normal distribution mean zero and variance  $\theta_2 = 0.3$ . The CS-I model constraints the regression coefficients in volatility of two components to be  $\boldsymbol{\beta}_1 = (-0.2, -0.05, -0.05)^\top$  and  $\boldsymbol{\beta}_2 = (1.4, -0.05, -0.05)^\top$ , i.e.,  $\beta_{11} = \beta_{21} = -0.05$  and  $\beta_{12} = \beta_{22} = -0.05$ . The CS-N model does not involve a mixture structure (simulation studies of the CS-N model have been reported in [Xie et al. \(2025\)](#) and are not presented here). The starting point  $x_0$  and the lower boundary  $\nu$  were set to be  $x_0 = 10$  and  $\nu = 3.9$ , respectively.

For each model, event gap times were simulated from the FHT distribution using the rejection sampling algorithm of [Xie et al. \(2025\)](#). The gap times were generated until the accumulated gap times reached or exceeded the follow-up time for subject  $i$ . Follow-up times were independently drawn from the empirical distribution observed in the motivating data. The group membership of each subject was then generated from a categorical distribution with the specified mixture weights. Different levels of sample sizes,  $n \in \{200, 500, 1000, 2000\}$  were considered. For each simulation setting, 100 datasets were generated.

For each dataset, Bayesian inference was performed using the prior distributions defined in Equation (3.3), with hyperparameters described in Section 3.2. For each dataset, an MCMC chain of 100,000 iterations was run, with the first 50,000 discarded as burn-in and the remaining iterations thinned by a factor of 100. Convergence was assessed using the Heidelberg–Welch diagnostic ([Heidelberg and Welch, 1983](#)) implemented in the R package CODA ([Plummer et al., 2006](#)). Posterior summaries and model selection criteria were computed from the resulting 500 MCMC samples.

Table 4 summarizes the estimation results for the three candidate models when the data were generated under the correct model specification. The bias, defined as the difference between the true parameter value and its point estimate (the posterior mean), is close to zero for all parameters at both sample sizes. The average posterior standard deviation closely

Table 4: Results of parameter estimation under correct specifications for three models with sample size  $n \in \{1000, 2000\}$ . SD, posterior standard deviation; ESD, empirical standard deviation; CR, coverage rate of 95% HPD credible interval.

Model	Para	True	$n = 1000$				$n = 2000$			
			Bias	SD	ESD	CR	Bias	SD	ESD	CR
CS-C-FV	$\alpha_0$	2.90	0.009	0.039	0.035	0.98	-0.001	0.027	0.025	0.98
	$\alpha_1$	0.20	0.003	0.044	0.043	0.96	0.001	0.031	0.027	0.97
	$\alpha_2$	-0.10	0.006	0.038	0.033	0.97	0.008	0.027	0.026	0.93
	$\beta_{10}$	-0.20	-0.055	0.117	0.107	0.95	-0.050	0.083	0.080	0.93
	$\beta_{11}$	-0.30	-0.016	0.099	0.091	0.95	-0.005	0.067	0.071	0.92
	$\beta_{12}$	-0.10	-0.003	0.087	0.081	0.97	-0.002	0.060	0.062	0.90
	$\beta_{20}$	1.40	-0.018	0.027	0.026	0.91	-0.013	0.020	0.019	0.90
	$\beta_{21}$	-0.05	0.001	0.022	0.019	0.96	-0.000	0.015	0.014	0.96
	$\beta_{22}$	-0.05	-0.001	0.021	0.018	0.98	-0.001	0.014	0.016	0.96
	$\rho_1$	0.40	-0.012	0.034	0.030	0.96	-0.012	0.026	0.024	0.90
	$\rho_2$	0.60	0.012	0.034	0.030	0.96	0.012	0.026	0.024	0.90
	$\theta_{11}$	0.50	0.030	0.143	0.095	0.98	-0.011	0.110	0.081	0.98
	$\theta_{12}$	0.10	0.013	0.014	0.012	0.89	0.008	0.010	0.008	0.88
	$\theta_2$	0.30	0.018	0.040	0.034	0.98	0.007	0.027	0.027	0.93
CS-I-FV	$\alpha_0$	2.90	0.010	0.039	0.035	0.99	-0.001	0.027	0.024	0.97
	$\alpha_1$	0.20	0.003	0.044	0.046	0.95	-0.001	0.031	0.028	0.95
	$\alpha_2$	-0.10	0.004	0.038	0.035	0.98	0.005	0.027	0.027	0.95
	$\beta_{10}$	-0.20	-0.056	0.118	0.086	0.96	-0.035	0.087	0.075	0.96
	$\beta_{20}$	1.40	-0.019	0.028	0.026	0.94	-0.012	0.021	0.019	0.97
	$\beta_1$	-0.05	-0.002	0.021	0.019	0.98	-0.001	0.015	0.014	0.94
	$\beta_2$	-0.05	-0.002	0.021	0.019	0.97	-0.002	0.014	0.015	0.95
	$\rho_1$	0.40	-0.015	0.036	0.027	0.96	-0.008	0.028	0.025	0.97
	$\rho_2$	0.60	0.015	0.036	0.027	0.96	0.008	0.028	0.025	0.97
	$\theta_{11}$	0.50	0.016	0.153	0.087	0.99	-0.006	0.119	0.085	0.97
	$\theta_{12}$	0.10	0.014	0.014	0.012	0.90	0.007	0.010	0.009	0.91
	$\theta_2$	0.30	0.019	0.040	0.036	0.97	0.007	0.027	0.028	0.91
CS-I	$\alpha_0$	2.90	0.007	0.040	0.036	0.98	0.002	0.028	0.027	0.93
	$\alpha_1$	0.20	0.003	0.045	0.046	0.94	0.001	0.031	0.027	0.98
	$\alpha_2$	-0.10	0.005	0.039	0.035	0.97	0.006	0.027	0.028	0.91
	$\beta_{10}$	-0.20	-0.012	0.056	0.096	0.99	-0.009	0.037	0.036	0.96
	$\beta_{20}$	1.40	-0.008	0.034	0.022	0.93	-0.005	0.015	0.014	0.93
	$\beta_1$	-0.05	-0.003	0.021	0.020	0.94	-0.001	0.014	0.013	0.95
	$\beta_2$	-0.05	-0.000	0.020	0.018	0.97	-0.002	0.014	0.015	0.92
	$\rho_1$	0.40	-0.002	0.022	0.040	0.95	-0.002	0.014	0.014	0.92
	$\rho_2$	0.60	0.002	0.022	0.040	0.95	0.002	0.014	0.014	0.92
	$\theta_1$	0.10	0.013	0.012	0.037	0.87	0.005	0.007	0.007	0.89
	$\theta_2$	0.30	0.018	0.040	0.035	0.97	0.007	0.028	0.029	0.90

matches the empirical standard deviation of the estimates, except for the frailty variance  $\theta_{11}$  or  $\theta_1$  across models; however, this agreement improves as the sample size increases from 1000 to 2000. The empirical coverage probabilities of the 95% highest posterior density (HPD) credible intervals are close to their nominal level for most parameters. Consistent performance is also observed at smaller sample sizes ( $n = 200$  and  $500$ ), with estimation accuracy and interval coverage remaining comparable to those at larger sample sizes. These results indicate that the estimation procedure is robust across a range of sample size settings. Additional details are provided in Section 4.1 of the Supplementary Materials.

We also evaluated the performance of the model comparison criteria based on a Monte Carlo sample size  $S = 1000$  to approximate the integral, with results summarized in Table 5 for sample sizes  $n = 200, 500, 1000$ , and  $2000$ . When either the CS-C-FV model or the CS-I model was the correct specification, both DIC and LPML show a fair level of accuracy in selecting the best model across all sample sizes, with selection frequencies improving as the sample size increases. When the CS-I-FV model was the correct specification, the frequencies of correctly selecting the model using DIC and LPML remained the highest among the candidates for  $n \geq 500$ , although they were comparatively lower than in the other two scenarios. For the smallest sample size  $n = 200$ , we observe that DIC and LPML tend to favor the simpler CS-I model when the true model is CS-I-FV, reflecting the limited ability of these criteria to distinguish between highly similar models in small samples, particularly when the models differ by only one random-effect variance parameter.

In addition to the above setting, we considered an alternative simulation scenario motivated by the observation that the treatment effects with opposite directions across latent components may be masked in a homogeneous model. In this scenario, the treatment effect was specified to be positive in one mixture component and negative in the other. Under this setting, we found that the proposed mixture model, CS-C-FV, was able to recover the component-specific treatment effects, whereas the CS-N frequently failed to detect a statistically significant treatment effect. Detailed simulation results for this scenario are provided

Table 5: Model comparison result with DIC and LPML with sample size  $n \in \{1000 \text{ and } 2000\}$ . Freq (%): frequency of the correct model being selected; Mean: average of the DIC or LPML.

True Model	Criterion	$n$	CS-C-FV		CS-I-FV		CS-I	
			Freq	Mean	Freq	Mean	Freq	Mean
CS-C-FV	DIC	200	54	12166.0	21	12167.5	24	12167.9
		500	75	29766.6	19	29770.6	6	29773.8
		1000	87	59511.9	8	59521.3	5	59526.6
		2000	100	119067.9	0	119087.3	0	119096.6
	LPML	200	40	-6086.5	26	-6086.6	35	-6086.7
		500	66	-14889.4	14	-14891.4	20	-14891.3
		1000	82	-29762.5	6	-29766.7	12	-29768.2
		2000	95	-59540.5	1	-59549.7	4	-59553.1
CS-I-FV	DIC	200	22	11996.6	37	11995.3	40	11995.9
		500	19	29518.4	49	29516.8	31	29518.7
		1000	15	58942.5	67	58993.3	18	58945.2
		2000	20	118024.3	68	118022.5	12	118031.4
	LPML	200	14	-6002.1	36	-6000.7	49	-6000.6
		500	14	-14763.6	46	-14762.3	39	-14762.4
		1000	11	-29477.0	60	-29502.4	29	-29477.5
		2000	20	-59017.1	67	-59016.4	13	-59019.5
CS-I	DIC	200	16	11703.7	36	11702.2	48	11702.4
		500	14	28701.5	25	28700.1	61	28699.3
		1000	2	57341.0	1	57338.7	97	57335.1
		2000	0	114703.4	3	114701.2	97	114697.1
	LPML	200	10	-5855.4	35	-5854.0	55	-5853.6
		500	14	-14354.7	19	-14354.1	67	-14352.8
		1000	3	-28675.6	5	-28674.7	92	-28672.4
		2000	1	-57356.3	6	-57355.2	93	-57352.9

in the Section 4.2 of the Supplementary Materials. Comparison of the computational time required for estimating the CS-C-FV and CS-N models across different sample sizes is presented in the Section 4.3 of the Supplementary Materials.

## 6 Discussion

Building on previous research that modeled recurrent hypoglycemic events using reflected Brownian motion to describe sequences hitting a lower boundary (Xie et al., 2025), we extended this framework to a finite mixture FHT model to better capture the unobserved heterogeneity in the patient population. This enhanced model assumes the patient-level frailty in volatility to be component-specific, allowing for distinct behavioral dynamics across patient subgroups. To further investigate the relationships between regression coefficients and frailty within the volatility context, we examined several reduced models, each representing different patterns of heterogeneity. Parameter estimation was carried out in a Bayesian framework. The effectiveness and reliability of two Bayesian model comparison criteria were evaluated through simulation studies, despite the high computational cost.

Applying these models to hypoglycemic events from motivating data enabled us to evaluate the proposed methodology in a realistic clinical trial setting and to explore the heterogeneity among patients. An important implication of modeling latent heterogeneity is that covariate effects may differ in both magnitude and direction across latent subgroups. In such settings, a homogeneous model that targets only a marginal effect may fail to detect statistically significant associations, even when strong but oppositely signed effects are present at the component level. This phenomenon is particularly relevant in biomedical applications, where treatment responses often vary substantially across unobserved risk groups. Motivated by that, we further investigated this scenario through an additional simulation study, which confirms that opposing component-specific effects can indeed result in significance being masked under a non-mixture model. Details of this simulation study are provided in the Supplementary Materials Section 4.2.

Several model assumptions warrant discussion. The introduction of an upper reflecting barrier imposes an upper limit on Brownian motion, which effectively prevents glucose levels from reaching infinite and eventually allows them to drop down. This assumption is reasonable for several considerations. First, the phenomenon of glycosuria occurs when glucose

levels in diabetic patients become so elevated that they surpass the kidneys' reabsorption capacity, leading to glucose being excreted in the urine and a subsequent reduction in blood glucose levels. Second, patients who consistently receive medication are able to maintain their glucose levels within a desired range. Although using a reflecting barrier to model the Brownian motion's reversal may not precisely depict the underlying mechanism of the glucose movement, it serves as a straightforward modeling approach that offers valuable insights into risk factors influencing glucose dynamics.

Sensitivity analyses on the choice of the Brownian motion reset point have been previously conducted by [Xie et al. \(2025\)](#), with the current model fixed at 10. These analyses showed that, although the estimated intercepts for the upper reflecting barrier and the volatility vary with the choice of starting point, the covariate effect estimates remain stable. In the present work, we further examined this issue by conducting an additional sensitivity analysis in which the starting point  $x_0$  was treated as a normal random variable with mean 10 and variance  $\theta_3$ . The resulting covariate effect estimates remain highly consistent with those from the main analysis. However, allowing the starting point to be random does not yield additional inferential insight beyond the fixed- $x_0$  specification and increases model complexity. Accordingly, we retain the CS-C-FV model with a fixed starting point as the primary analysis, and report the randomized- $x_0$  specification only as a sensitivity analysis. Detailed results are provided in Section 3 of the Supplementary Materials.

Enhancing the current model is possible from several perspectives, but each entails substantial increases in complexity and computational demands. Allowing frailty to arise from different distributions would provide greater model flexibility, yet it would also introduce a large number of latent variables. In a Bayesian framework, these latent variables are treated as parameters, substantially increasing the computational burden. The number of components in the mixture model, currently fixed at two, could be evaluated using model comparison criteria; However, adding additional mixture components (e.g.,  $K = 3$ ) to the proposed model, which already includes two subject-level random parameters, one of which

is component-specific, would substantially increase the number of latent variables. This increase in the number of parameters would further complicate the model and may lead to weak identifiability, poor MCMC mixing in finite samples, and longer computational time. For further exploration, Dirichlet Process Mixture Models (Race and Pennell, 2021) may provide a viable alternative by avoiding the need to fix the number of mixture components a priori. We have also explored linking covariates to the mixture weights to classify patients into distinct groups, with the goal of generating insights for personalized medicine. Although this approach theoretically enhances the model’s utility, in practice it complicated the model structure and made MCMC convergence more difficult in our studies.

## A FHT Distribution of Reflected Brownian Motion

For a no-drift Brownian motion  $X(t)$  with volatility  $\sigma$ , let  $\kappa$  be the upper reflection barrier  $\kappa > \nu$  and  $\nu$  be the lower boundary. Suppose that  $X(0) = x_0 \in [\nu, \kappa]$  is the starting point, the first time when  $X(t)$  hits  $\nu$  is  $\tau := \inf\{t > 0; X(t) = \nu\}$ . The density and distribution function of  $\tau$  are, respectively (Hu et al., 2012),

$$f(t|x_0, \nu, \kappa, \sigma) = \sum_{n=1}^{\infty} c_n \lambda_n e^{-\lambda_n t}, \quad t > 0, \quad (\text{A.1})$$

$$F(t|x_0, \nu, \kappa, \sigma) = 1 - \sum_{n=1}^{\infty} c_n e^{-\lambda_n t}, \quad t > 0, \quad (\text{A.2})$$

where for  $n = 1, 2, \dots$ ,

$$\lambda_n = \frac{(2n-1)^2 \sigma^2 \pi^2}{8(\kappa - \nu)^2}, \text{ and } c_n = \frac{(-1)^{n+1} 4}{(2n-1)\pi} \cos\left(\frac{(2n-1)\pi(\kappa - x_0)}{2(\kappa - \nu)}\right).$$

Note that  $0 < \lambda_1 < \lambda_2 < \dots$ ,  $\lambda_n \rightarrow \infty$ , and  $\sum_{n=1}^{\infty} c_n = 1$ . Both functions involve infinite series, which present challenges to accurate evaluation of the log-likelihood and efficient design of random number generation. To maintain numerical accuracy in implementing the

density and distribution functions, we do not impose a fixed number of terms  $N$  on the summation. Instead, the infinite series is evaluated using a tolerance-based stopping rule, where the summation is terminated when the ratio of the current term to the cumulative sum is less than or equal to a prespecified threshold, set to  $10^{-10}$  in this study. A comprehensive sensitivity analysis regarding the choice of tolerance in the evaluation of the density and survival probability, as well as parameter estimation in data application, is provided in Supplementary Materials Section 3.3.

An efficient rejection algorithm to sample random number from the distribution has been proposed by [Xie et al. \(2025\)](#). The implementation has been released in a R package `reflbrown` ([Xie and Yan, 2024](#)).

## References

- Aalen, O. O. and Gjessing, H. K. (2001), “Understanding the shape of the hazard rate: A process point of view (with comments and a rejoinder by the authors),” *Statistical Science*, 16, 1–22.
- Buse, J. B., Wolffenbuttel, B. H., Herman, W. H., Shemonsky, N. K., Jiang, H. H., Fahrbach, J. L., Scism-Bacon, J. L., and Martin, S. A. (2009), “Durability of Basal versus Lispro Mix 75/25 Insulin Efficacy (Durable) Trial 24-Week Results: Safety and Efficacy of Insulin Lispro Mix 75/25 Versus Insulin Glargine Added to Oral Antihyperglycemic Drugs in Patients with Type 2 Diabetes,” *Diabetes Care*, 32, 1007–1013.
- Charles-Nelson, A., Katsahian, S., and Schramm, C. (2019), “How to Analyze and Interpret Recurrent Events Data in the Presence of a Terminal Event: An Application on Readmission after Colorectal Cancer Surgery,” *Statistics in Medicine*, 38, 3476–3502.
- Cook, R. J. and Lawless, J. F. (2007), *The Statistical Analysis of Recurrent Events*, New York: Springer.

- Cryer, P. E., Davis, S. N., and Shamoon, H. (2003), “Hypoglycemia in Diabetes,” *Diabetes Care*, 26, 1902–1912.
- de Valpine, P., Turek, D., Paciorek, C., Anderson-Bergman, C., Temple Lang, D., and Bodik, R. (2017), “Programming With Models: Writing Statistical Algorithms for General Model Structures with NIMBLE,” *Journal of Computational and Graphical Statistics*, 26, 403–413.
- Dey, D. K., Chen, M.-H., and Chang, H. (1997), “Bayesian Approach for Nonlinear Random Effects Models,” *Biometrics*, 53, 1239–1252.
- Economou, P., Malefaki, S., and Caroni, C. (2015), “Bayesian Threshold Regression Model with Random Effects for Recurrent Events,” *Methodology and Computing in Applied Probability*, 17, 871–898.
- Fu, H., Luo, J., and Qu, Y. (2016), “Hypoglycemic Events Analysis via Recurrent Time-to-Event (HEART) Models,” *Journal of Biopharmaceutical Statistics*, 26, 280–298.
- Geisser, S. and Eddy, W. F. (1979), “A Predictive Approach to Model Selection,” *Journal of the American Statistical Association*, 74, 153–160.
- Gelfand, A. E. and Dey, D. K. (1994), “Bayesian Model Choice: Asymptotics and Exact Calculations,” *Journal of the Royal Statistical Society: Series B (Methodological)*, 56, 501–514.
- Heidelberger, P. and Welch, P. D. (1983), “Simulation Run Length Control in the Presence of an Initial Transient,” *Operations Research*, 31, 1109–1144.
- Hofert, M., Kojadinovic, I., Mächler, M., and Yan, J. (2018), *Elements of Copula Modeling with R*, Springer.
- Hu, Q., Wang, Y., and Yang, X. (2012), “The Hitting Time Density for a Reflected Brownian Motion,” *Computational Economics*, 40, 1–18.

- Jiang, R., Law, E., Zhou, Z., Yang, H., Wu, E. Q., and Seifeldin, R. (2018), “Clinical Trajectories, Healthcare Resource Use, and Costs of Diabetic Nephropathy among Patients with Type 2 Diabetes: A Latent Class Analysis,” *Diabetes Therapy*, 9, 1021–1036.
- Lee, M.-L. T. (2019), “A Survey of Threshold Regression for Time-to-Event Analysis and Applications,” *Taiwanese Journal of Mathematics*, 23, 293–305.
- Lee, M.-L. T., Chang, M., and Whitmore, G. (2008), “A threshold regression mixture model for assessing treatment efficacy in a multiple myeloma clinical trial,” *Journal of Biopharmaceutical Statistics*, 18, 1136–1149.
- Lee, M.-L. T. and Whitmore, G. A. (2003), “First Hitting Time Models for Lifetime Data,” in *Advances in Survival Analysis*, eds. Balakrishnan, N. and Rao, C., Elsevier, vol. 23 of *Handbook of Statistics*, pp. 537–543.
- (2006), “Threshold Regression for Survival Analysis: Modeling Event Times by a Stochastic Process Reaching a Boundary,” *Statistical Science*, 21, 501–513.
- Ma, H., Peng, L., Huang, C.-Y., and Fu, H. (2021), “Heterogeneous Individual Risk Modelling of Recurrent Events,” *Biometrika*, 108, 183–198.
- Malefaki, S., Economou, P., and Caroni, C. (2015), “Modelling times between events with a cured fraction using a first hitting time regression model with individual random effects,” in *Theory and Practice of Risk Assessment: ICRA 5, Tomar, Portugal, 2013*, eds. Kitsos, C., Oliveira, T., Rigas, A., and Gulati, S., Springer, pp. 45–65.
- Papastamoulis, P. (2016), “label.switching: An R package for dealing with the label switching problem in MCMC outputs,” *Journal of Statistical Software*, 69, 1–24.
- Pennell, M. L., Whitmore, G., and Ting Lee, M.-L. (2010), “Bayesian Random-Effects Threshold Regression with Application to Survival Data with Nonproportional Hazards,” *Biostatistics*, 11, 111–126.

- Plummer, M., Best, N., Cowles, K., and Vines, K. (2006), “CODA: Convergence Diagnosis and Output Analysis for MCMC,” *R News*, 6, 7–11.
- Qu, H., Shewchuk, R. M., Richman, J., Andreae, L. J., and Safford, M. M. (2022), “Identifying Patient Profiles for Developing Tailored Diabetes Self-management Interventions: A Latent Class Cluster Analysis,” *Risk Management and Healthcare Policy*, 1055–1063.
- Race, J. A. and Pennell, M. L. (2021), “Semi-parametric Survival Analysis via Dirichlet Process Mixtures of the First Hitting Time Model,” *Lifetime Data Analysis*, 27, 177–194.
- Seaquist, E. R., Anderson, J., Childs, B., Cryer, P., Dagogo-Jack, S., Fish, L., Heller, S. R., Rodriguez, H., Rosenzweig, J., and Vigersky, R. (2013), “Hypoglycemia and Diabetes: A Report of a Workgroup of the American Diabetes Association and the Endocrine Society,” *Diabetes Care*, 36, 1384–1395.
- Spiegelhalter, D. J., Best, N. G., Carlin, B. P., and Van Der Linde, A. (2002), “Bayesian Measures of Model Complexity and Fit,” *Journal of the Royal Statistical Society: Series B (Statistical Methodology)*, 64, 583–639.
- Stephens, M. (2000), “Dealing with label switching in mixture models,” *Journal of the Royal Statistical Society: Series B (Statistical Methodology)*, 62, 795–809.
- Whitmore, G. A. (1986), “First-passage-time models for duration data: Regression structures and competing risks,” *Journal of the Royal Statistical Society: Series D (The Statistician)*, 35, 207–219.
- Whitmore, G. A. and Su, Y. (2007), “Modeling Low Birth Weights Using Threshold Regression: Results for US Birth Data,” *Lifetime Data Analysis*, 13, 161–190.
- Xie, Y., Fu, H., Huang, Y., Pozdnyakov, V., and Yan, J. (2025), “Recurrent Events Modeling based on a Reflected Brownian Motion with Application to Hypoglycemia,” *Biostatistics*, 26, kxae053.

Xie, Y. and Yan, J. (2024), “reflbrown: Recurrent Event Modeling based on First Hitting Time of Reflected Brownian Motion,” <https://github.com/YingfaX/reflbrown>, R package version 0.1.0.

# Supplementary Material for “Unobserved Heterogeneity in Threshold Regression Based on the Hitting Times of a Reflected Brownian Motion for Recurrent Hypoglycemia”

<sup>1</sup>, Yingfa Xie<sup>1,3</sup>, Haoda Fu<sup>2</sup>, Yuan Huang <sup>\*3</sup> and Jun Yan<sup>1</sup>

<sup>1</sup>*Department of Statistics, University of Connecticut*

<sup>2</sup>*Indiana University School of Medicine*

<sup>3</sup>*Department of Biostatistics, Yale School of Public Health*

## 1 Additional Data Summary

Table 1 summarizes additional descriptive statistics of the continuous covariates in the analysis data.

## 2 MCMC Convergence

The traceplots of the parameters of the component-specific coefficient and frailty variance (CS-C-FV) model are shown in Figure 1 (corresponding to the parameters in upper reflection barrier  $\kappa$ ), 2 (corresponding to the parameters in volatility  $\sigma$  of the first component), and 3 (corresponding to the parameters in volatility  $\sigma$  of the second component). Two MCMC chains for each parameter are run with different initial values. The traceplots show that two MCMC chains mix well, indicating that the MCMCs have converged.

Additional, we compute the Gelman–Rubin (Gelman and Rubin, 1992) potential scale reduction factor using multiple chains with R package coda (Plummer et al., 2006), and all parameters have values close to 1, indicating good convergence. We report the effective sample size (ESS) and the corresponding Monte Carlo standard error (MCSE) for all model parameters. The ESS values are sufficiently large (relatively small for some component-specific parameters), while the MCSE values are small relative to the posterior standard deviations, suggesting that Monte Carlo error has negligible impact on the posterior summaries. These diagnostics collectively indicate satisfactory convergence of the MCMC algorithm. The results are summarized in Table 2.

---

\*Email address: yuan.huang@yale.edu; corresponding author

Table 1: Descriptive statistics of the continuous covariates. BMI, body mass index; BP, blood pressure; Min, minimum; Max, maximum; SD, standard deviation.

Covariate	Min	Median	Max	Mean	SD
<i>Glargine</i>					
Fasting glucose (mmol/l)	1.28	10.37	25.96	10.81	3.59
Adiponectin ( $\mu\text{g/ml}$ )	0.01	5.64	48.71	6.89	5.18
Fasting insulin (mIU/L)	0.18	7.81	142.68	10.47	10.90
Height (cm)	124.25	166.14	197.04	166.19	10.91
BMI ( $\text{kg/m}^2$ )	15.88	31.40	53.96	31.74	6.16
Diastolic BP (mmHg)	48.16	78.73	116.30	78.23	9.40
Systolic BP (mmHg)	89.17	130.23	196.67	131.41	15.96
Heart rate (beats per minute)	50.40	76.84	121.05	76.87	9.81
Duration diabetes (years)	0.04	8.27	36.82	9.53	5.98
<i>LM 75/25</i>					
Fasting glucose (mmol/l)	0.23	10.55	24.47	10.78	3.83
Adiponectin ( $\mu\text{g/ml}$ )	0.04	5.45	49.01	7.06	5.82
Fasting insulin (mIU/L)	0.18	8.16	89.85	10.29	8.49
Height (cm)	139.93	166.86	198.09	166.77	10.55
BMI ( $\text{kg/m}^2$ )	16.11	31.16	62.62	31.66	6.23
Diastolic BP (mmHg)	45.01	78.71	111.57	78.28	9.53
Systolic BP (mmHg)	47.26	129.77	191.88	131.71	16.30
Heart rate (beats per minute)	43.86	76.39	119.29	76.70	9.82
Duration diabetes (years)	0.03	8.94	39.48	10.00	6.34

### 3 Sensitivity Analysis

#### 3.1 Sensitivity Analysis with a Random Starting Point

We investigated an extension of the proposed framework by allowing the starting point  $x_0$  to be random. In the original specification described in the main manuscript, the starting point  $x_0$  is fixed at 10. To assess the sensitivity of the proposed model to this assumption, we consider an alternative specification in which  $x_0$  is treated as a normal random variable by introducing a subject-level random effect with a known mean 10 and variance  $\theta_3$ . This study allows us to examine whether randomness in the starting point materially affects the estimation of covariate effects compared with the fixed starting point setting used in the main analysis.

As shown in Figure 4, the estimated covariate effects from the CS-C-FV model with a random starting point are highly consistent with those obtained under the fixed- $x_0$  specification. The overall significance pattern of the covariate effects remains unchanged, and other key parameter estimates are likewise very similar. The estimated frailty standard deviation for the starting point is 0.53, corresponding to an estimated variance of  $\theta_3 = 0.28$ . Taken together, these results indicate that the main findings of the paper are robust to allowing subject-level variation in  $x_0$ , and that this additional flexibility does not materially alter

Table 2: Convergence diagnostics for the CS-C-FV model. For each parameter, the Gelman–Rubin potential scale reduction factor ( $\hat{R}$ ), effective sample size (ESS), and Monte Carlo standard error (MCSE) are reported for the posterior samples.

Covariates	Volatility						Upper reflection barrier		
	Group 1			Group 2			$\hat{R}$	ESS	MCSE
	$\hat{R}$	ESS	MCSE	$\hat{R}$	ESS	MCSE			
Intercept	1.0064	193	0.0093	1.0010	742	0.0010	1.0192	967	0.0020
Fasting glucose	1.0019	1015	0.0016	1.0025	3411	0.0002	1.0039	4359	0.0005
Adiponectin	1.0012	671	0.0026	1.0000	2822	0.0002	1.0038	3142	0.0005
Fasting insulin	1.0003	755	0.0020	1.0001	2844	0.0003	1.0020	3286	0.0006
Height	1.0001	1098	0.0015	1.0015	3374	0.0002	1.0011	3963	0.0005
BMI	1.0048	809	0.0021	1.0001	3287	0.0002	1.0011	3322	0.0006
Diastolic BP	1.0028	810	0.0022	1.0019	2556	0.0003	1.0020	2802	0.0007
Systolic BP	1.0012	776	0.0023	1.0010	2564	0.0003	1.0008	3259	0.0005
Heart rate	1.0139	772	0.0022	1.0003	3364	0.0002	1.0002	4130	0.0004
Duration diabetes	1.0012	874	0.0016	1.0048	3567	0.0002	1.0008	4233	0.0004
LM	1.0084	547	0.0047	1.0006	1681	0.0006	1.0005	2025	0.0013
tzd-only	1.0004	620	0.0078	1.0002	2625	0.0012	1.0079	4060	0.0023
sulf-only	1.0053	303	0.0069	1.0000	1089	0.0008	1.0228	1157	0.0019
Frailty std	1.0262	890	0.0027	1.0083	1119	0.0002	1.0014	3463	0.0007
Mixture Weight	1.0073	776	0.0008	1.0073	776	0.0008			

inference for the current dataset.

Because introducing a random starting point does not provide additional inferential insight beyond the fixed- $x_0$  specification while increasing model complexity, we retain the fixed- $x_0$  CS-C-FV model as the primary analysis in the manuscript. The randomized- $x_0$  extension is therefore reported as a sensitivity analysis to demonstrate the robustness of the proposed method to this modeling assumption, rather than as the main modeling framework.

### 3.2 Sensitivity Analysis with Initial Values for Mixture Weights

To assess the sensitivity of the inferred mixture component assignments to the choice of starting values, we conducted a sensitivity analysis using alternative initial values for the mixture weights. In the primary MCMC run, the mixture weights  $\boldsymbol{\rho}$  were initialized at (0.4, 0.6). Four additional runs were performed with alternative starting values: (0.2, 0.8), (0.6, 0.4), (0.8, 0.2), and (0.5, 0.5), representing both balanced and highly unbalanced initial configurations. Across all runs, the posterior estimates of  $\boldsymbol{\rho}$  were nearly identical, indicating that the inference is robust to the choice of starting values.

For each run, posterior samples of the latent class indicators were obtained from the MCMC output. For each subject, we estimated the posterior probability of belonging to each mixture component by calculating the proportion of MCMC iterations in which the subject was assigned to that component. Hard class assignments were then derived by

Table 3: Sensitivity of class assignments to alternative starting values for the mixture weights. Entries  $i \rightarrow j$  represent the number of subjects assigned to class  $i$  in the primary run and class  $j$  in the alternative run. Agreement denotes the proportion of subjects with identical class assignments across runs; PS: primary setting; AS: alternative setting; Est.: estimated.

Setting	Starting Weights	Est. Weights	1 $\rightarrow$ 1	1 $\rightarrow$ 2	2 $\rightarrow$ 1	2 $\rightarrow$ 2	Agreement
PS	(0.4, 0.6)	(0.440, 0.560)	-	-	-	-	-
AS 1	(0.2, 0.8)	(0.440, 0.560)	845	2	3	1093	0.997
AS 2	(0.6, 0.4)	(0.443, 0.557)	846	1	7	1089	0.996
AS 3	(0.8, 0.2)	(0.438, 0.562)	844	3	1	1095	0.998
AS 4	(0.5, 0.5)	(0.439, 0.561)	842	5	3	1093	0.996

assigning each subject to the component with the larger posterior probability (i.e., using 0.5 as the cut-off point).

We compared the resulting hard class assignments between the alternative runs and the primary run. Table 3 presents the cross classification of assignments between the primary run and each alternative run. The table entries represent the number of subjects assigned to class  $i$  in the primary run and class  $j$  in the alternative run. The agreement rates were very high ( $\geq 0.996$ ), indicating that the inferred class assignments were stable across different starting values.

### 3.3 Sensitivity Analysis for Truncation Level in Distribution Implementation

Additional sensitivity analyses for different tolerance levels in the implementation of the reflected Brownian motion first hitting time density and distribution functions (Hu et al., 2012) were conducted. The tolerance parameter controls the stopping rule for the infinite series evaluation, where the summation is terminated when the ratio of the current term to the cumulative sum is less than or equal to a prespecified threshold.

We first examined the impact of the tolerance level on the numerical evaluation of the FHT density and survival probability. Specifically, we considered tolerance levels 0,  $10^{-6}$ ,  $10^{-8}$ ,  $10^{-10}$ , and  $10^{-12}$ , where tolerance = 0 serves as a practically untruncated reference. Figure 5 illustrates the absolute differences in log-likelihood evaluation relative to this reference across a range of representative parameter settings and gap times. The differences are extremely small across all settings. Even for the relatively coarse tolerance  $10^{-6}$ , the differences are at the  $10^{-6}$  scale or smaller, and are primarily observed when the gap time is close to zero. As the gap time increases, the differences rapidly diminish and become negligible. For tolerances  $10^{-8}$  and below, the results are virtually indistinguishable from the reference, indicating that the stopping rule introduces minimal numerical error.

To assess the sensitivity of the estimation results to this numerical criterion, we further repeated the data analysis under several alternative tolerance levels. In addition to the primary setting ( $10^{-10}$ ), we considered three alternative values: ( $10^{-6}$ ), ( $10^{-8}$ ), and ( $10^{-12}$ ). These settings represent both looser and stricter stopping criteria for the infinite series

evaluation.

Figure 6 compares the parameter estimates and their corresponding HPD intervals obtained under these different tolerance levels. The results show that the estimates remain highly consistent across all settings. Both the point estimates and the confidence intervals exhibit negligible variation when the tolerance parameter changes, indicating that the numerical implementation of the infinite series is stable with respect to the choice of truncation criterion.

## 4 Additional Simulation Results

### 4.1 Smaller Sample Sizes

Additional simulation studies are presented to examine performance at smaller sample sizes. The main manuscript reports results for  $n \in 1000, 2000$ , whereas results for  $n \in 200, 500$  are reported here.

Table 4 shows that the estimation procedure remains stable at these sample sizes. Parameter bias is small, estimated standard deviations are close to the corresponding empirical standard deviations, and coverage probabilities are close to the nominal level.

### 4.2 Opposite Effect Directions in Mixture Components

We conducted a simulation study to assess whether a non mixture model, CS-N, can detect a treatment effect when the true treatment effects have opposite signs across mixture components. Specifically, we set the component specific treatment coefficients to  $\beta_{11} = -0.4$  and  $\beta_{21} = 0.08$ , with mixing proportions  $(\pi_1, \pi_2) = (0.4, 0.6)$ . The true values of other model parameters are given in Table 5. For each of 100 replicates, we generated data from the proposed mixture model, CS-C-FV, fitted the mixture model to obtain estimates and 95% HPD credible intervals for  $\beta_{11}$  and  $\beta_{21}$ , and also fitted the non mixture model, CS-N, to obtain an estimate and 95% HPD credible intervals for the treatment coefficient  $\beta_1$ . To visualize the results, we used forest plots showing replicate level point estimates and HPD credible intervals, with replicates sorted within each parameter panel.

Figure 7 summarizes the HPD credible intervals of treatment effect estimates and corresponding 95% HPD credible intervals across simulation replicates. When fitting the CS-C-FV, the component specific treatment effects were detected with high empirical power. Specifically, the treatment effect  $\beta_{11}$  was statistically significant in 88 out of 100 replicates (power = 0.88), and  $\beta_{21}$  was significant in 86 out of 100 replicates (power = 0.86), with HPD credible intervals concentrated around their respective true values.

In contrast, the CS-N model exhibited substantially lower power for detecting the treatment effect. The estimated coefficient  $\beta_1$  was statistically significant in only 13 out of 100 replicates (power = 0.13), with the majority of HPD credible intervals overlapping zero. This pronounced difference reflects the cancellation of oppositely signed component specific effects when aggregated into a single marginal effect, highlighting the limitation of the non mixture model in the presence of heterogeneous treatment responses.

Table 4: Results of parameter estimation under correct specifications for three models with sample size  $n \in \{200, 500\}$ . SD, posterior standard deviation; ESD, empirical standard deviation; CR, coverage rate of 95% highest posterior density (HPD) credible interval.

Model	Para	True	$n = 200$				$n = 500$				
			Bias	SD	ESD	CR	Bias	SD	ESD	CR	
CS-C-FV	$\alpha_0$	2.90	-0.025	0.091	0.089	0.94	-0.015	0.056	0.056	0.94	
	$\alpha_1$	0.20	-0.034	0.104	0.108	0.90	-0.016	0.063	0.065	0.89	
	$\alpha_2$	-0.10	0.019	0.087	0.091	0.90	0.005	0.054	0.053	0.93	
	$\beta_{10}$	-0.20	0.302	0.430	0.549	0.90	0.031	0.167	0.169	0.94	
	$\beta_{11}$	-0.30	0.055	0.365	0.307	0.93	-0.010	0.136	0.149	0.90	
	$\beta_{12}$	-0.10	0.080	0.323	0.313	0.96	0.027	0.122	0.131	0.93	
	$\beta_{20}$	1.40	0.040	0.069	0.080	0.88	0.013	0.041	0.045	0.91	
	$\beta_{21}$	-0.05	0.005	0.050	0.041	0.97	-0.003	0.030	0.031	0.94	
	$\beta_{22}$	-0.05	0.000	0.049	0.051	0.95	-0.008	0.029	0.029	0.95	
	$\rho_1$	0.40	0.041	0.076	0.071	0.87	0.004	0.052	0.053	0.91	
	$\rho_2$	0.60	-0.041	0.076	0.071	0.87	-0.004	0.052	0.053	0.91	
	$\theta_{11}$	0.50	0.023	0.369	0.248	0.97	0.020	0.203	0.182	0.89	
	$\theta_{12}$	0.10	-0.025	0.040	0.047	0.86	-0.004	0.021	0.021	0.94	
	$\theta_2$	0.30	-0.028	0.098	0.106	0.90	-0.012	0.058	0.063	0.93	
CS-I-FV	$\alpha_0$	2.90	-0.023	0.092	0.086	0.94	-0.013	0.056	0.056	0.93	
	$\alpha_1$	0.20	-0.025	0.104	0.109	0.92	-0.013	0.063	0.066	0.91	
	$\alpha_2$	-0.10	0.016	0.088	0.093	0.89	0.003	0.054	0.056	0.93	
	$\beta_{10}$	-0.20	0.047	0.281	0.291	0.96	0.010	0.163	0.172	0.94	
	$\beta_{20}$	1.40	0.011	0.065	0.064	0.91	0.011	0.042	0.046	0.91	
	$\beta_1$	-0.05	0.006	0.048	0.041	0.98	-0.001	0.030	0.032	0.93	
	$\beta_2$	-0.05	0.003	0.046	0.046	0.96	-0.006	0.028	0.029	0.96	
	$\rho_1$	0.40	0.008	0.081	0.063	0.98	0.001	0.055	0.061	0.91	
	$\rho_2$	0.60	-0.008	0.081	0.063	0.98	-0.001	0.055	0.061	0.91	
	$\theta_{11}$	0.50	0.001	0.335	0.227	0.95	0.026	0.215	0.192	0.90	
	$\theta_{12}$	0.10	-0.008	0.035	0.034	0.96	-0.003	0.021	0.023	0.93	
	$\theta_2$	0.30	-0.029	0.100	0.108	0.89	-0.012	0.058	0.063	0.93	
	CS-I	$\alpha_0$	2.90	-0.024	0.093	0.091	0.95	-0.012	0.057	0.059	0.94
		$\alpha_1$	0.20	-0.028	0.107	0.106	0.93	-0.014	0.064	0.067	0.90
$\alpha_2$		-0.10	0.014	0.090	0.096	0.92	0.004	0.055	0.056	0.94	
$\beta_{10}$		-0.20	0.011	0.119	0.115	0.97	0.004	0.073	0.074	0.94	
$\beta_{20}$		1.40	-0.007	0.048	0.046	0.97	0.001	0.030	0.034	0.92	
$\beta_1$		-0.05	0.006	0.046	0.036	0.99	-0.002	0.029	0.030	0.90	
$\beta_2$		-0.05	0.001	0.044	0.046	0.94	-0.006	0.027	0.028	0.95	
$\rho_1$		0.40	0.004	0.044	0.035	0.95	-0.000	0.028	0.029	0.95	
$\rho_2$		0.60	-0.004	0.044	0.035	0.95	0.000	0.028	0.029	0.95	
$\theta_1$		0.10	-0.006	0.025	0.025	0.95	-0.002	0.015	0.013	0.97	
$\theta_2$		0.30	-0.032	0.101	0.114	0.89	-0.013	0.059	0.064	0.93	

Table 5: True values in CS-C-FV model

Component	Parameter	True Value
Reflecting bound	$\alpha_0$	2.90
	$\alpha_1$	0.20
	$\alpha_2$	-0.10
Volatility Component 1	$\beta_{10}$	-0.20
	$\beta_{11}$	-0.40
	$\beta_{12}$	-0.05
Volatility Component 2	$\beta_{20}$	1.40
	$\beta_{21}$	0.08
	$\beta_{22}$	-0.05
Mixture Weight	$\rho_1$	0.40
	$\rho_2$	0.60
Frailty Variance	$\theta_{11}$	0.50
	$\theta_{12}$	0.10
	$\theta_2$	0.30

### 4.3 Model Estimation Runtime

Furthermore, we report the MCMC runtime (in hours) across 100 simulation replicates for each model at different sample sizes ( $n = 200, 500, 1000$ ), as shown in Figure 8. The reported runtimes correspond solely to posterior sampling and exclude the computation of model comparison criteria. Overall, the CS-C-FV model requires longer computational time than the CS-N model, with the difference becoming more pronounced as the sample size increases, as expected given the additional model complexity of the CS-C-FV specification.

Computing the model comparison criteria incurs substantially greater computational cost, as it requires numerical integration via Monte Carlo approximation at each posterior iteration. In our experiments, the additional runtime associated with evaluating these criteria is approximately 2.5 times the MCMC runtime.

## 5 Computational Implementation

Our implementation of the CS-C-FV model uses the R package NIMBLE (de Valpine et al., 2017). After defining the model in NIMBLE code, we adopt the most straightforward approach for running Markov chain Monte Carlo (MCMC) sampling in NIMBLE by using the `nimbleMCMC()` function. This single function is used to define the underlying model and its corresponding MCMC algorithm, compile both components, run the MCMC procedure, and return posterior samples (de Valpine et al., 2025). NIMBLE automatically assigns sampler types based on model structure, using Gibbs samplers when conjugacy is available and Metropolis–Hastings or other generic samplers otherwise.

In our proposed model, the parameters of the FHT distribution of the reflected Brownian motion do not have conjugate priors, so NIMBLE assigns a random-walk sampler by default.

Specifically, this is an adaptive Metropolis–Hastings random-walk sampler with a univariate normal proposal distribution (de Valpine et al., 2025, see Section 7.2.2.1 for details). NIMBLE also allows users to customize the MCMC configuration when needed.

Label switching is a well-known challenge in MCMC estimation for Bayesian finite mixture models. We address the label switching issue during the MCMC sampling process by imposing an identifiability constraint on the component-specific parameters. Specifically, we constrain the intercepts of the component-specific volatility parameters  $\sigma$  such that  $\beta_{10} \leq \beta_{20}$ . This ordering constraint ensures that the two mixture components remain identifiable throughout the MCMC sampling. This technique can be implemented with NIMBLE (de Valpine et al., 2025, see Section 5.2.7.3 for details).

The implementation of the model with NIMBLE code has been provided in a separately R file.

## References

- de Valpine, P., Paciorek, C., Turek, D., Michaud, N., Anderson-Bergman, C., Obermeyer, F., Wehrhahn Cortes, C., Rodríguez, A., Temple Lang, D., and Paganin, S. (2025), “NIMBLE User Manual,” <https://r-nimble.org>, R package manual version 1.4.0.
- de Valpine, P., Turek, D., Paciorek, C., Anderson-Bergman, C., Temple Lang, D., and Bodik, R. (2017), “Programming With Models: Writing Statistical Algorithms for General Model Structures with NIMBLE,” *Journal of Computational and Graphical Statistics*, 26, 403–413.
- Gelman, A. and Rubin, D. B. (1992), “Inference from iterative simulation using multiple sequences,” *Statistical science*, 7, 457–472.
- Hu, Q., Wang, Y., and Yang, X. (2012), “The Hitting Time Density for a Reflected Brownian Motion,” *Computational Economics*, 40, 1–18.
- Plummer, M., Best, N., Cowles, K., and Vines, K. (2006), “CODA: Convergence Diagnosis and Output Analysis for MCMC,” *R News*, 6, 7–11.

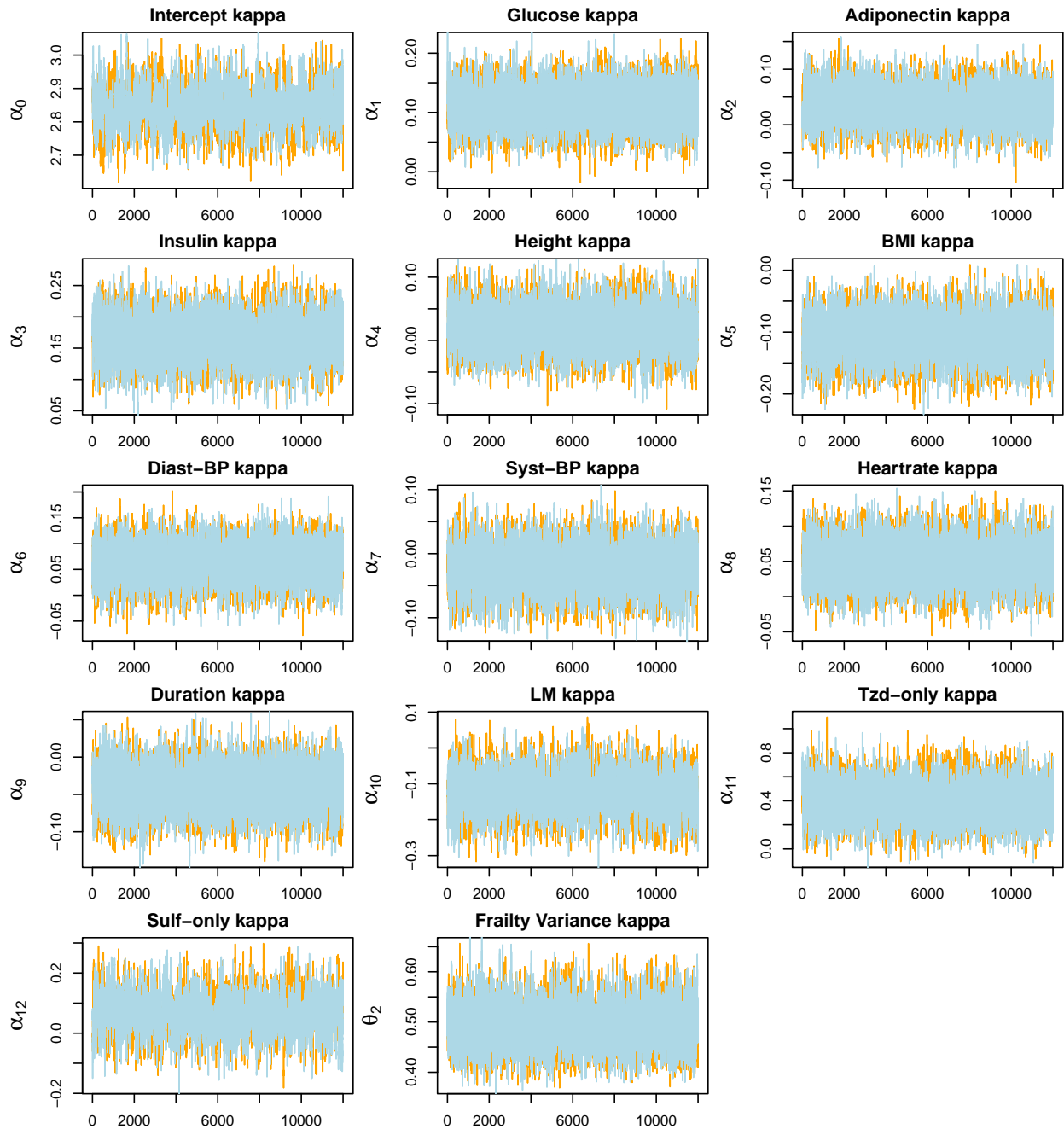


Figure 1: Traceplots of the parameters in upper reflection barrier of the CS-C-FV model

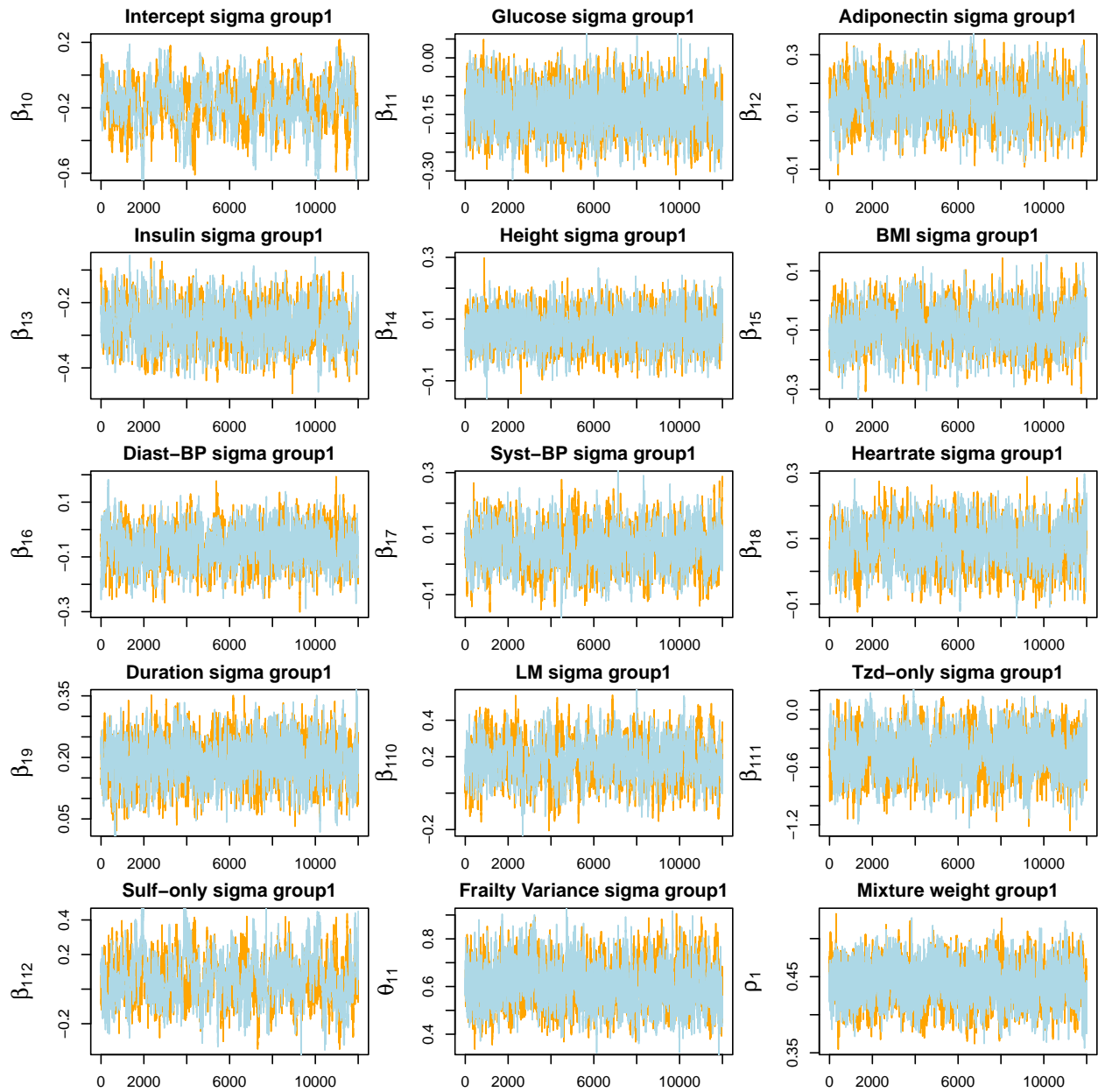


Figure 2: Traceplots of the parameters in volatility of the first component of the CS-C-FV model

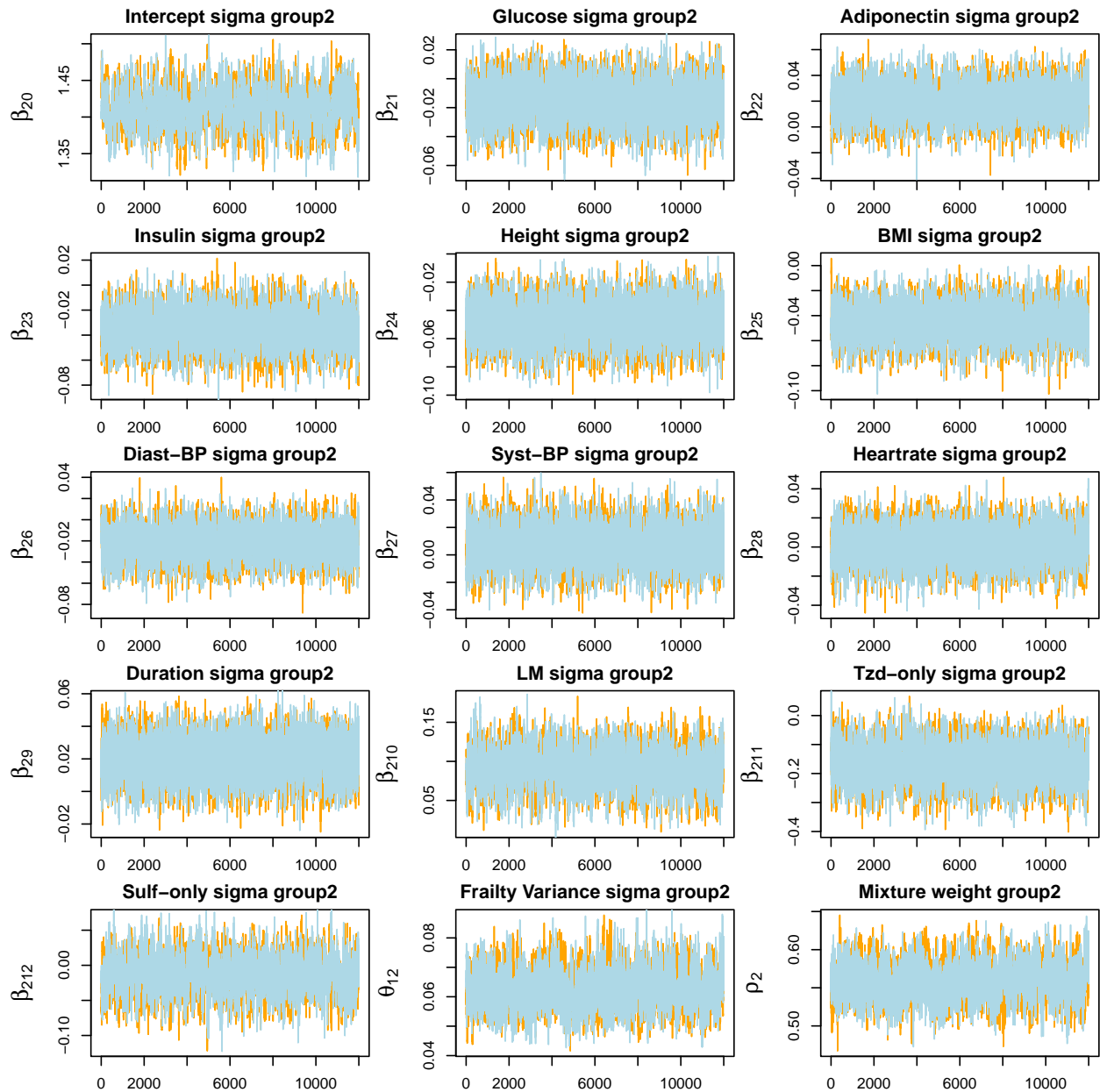


Figure 3: Traceplots of the parameters in volatility of the second component of the CS-C-FV model

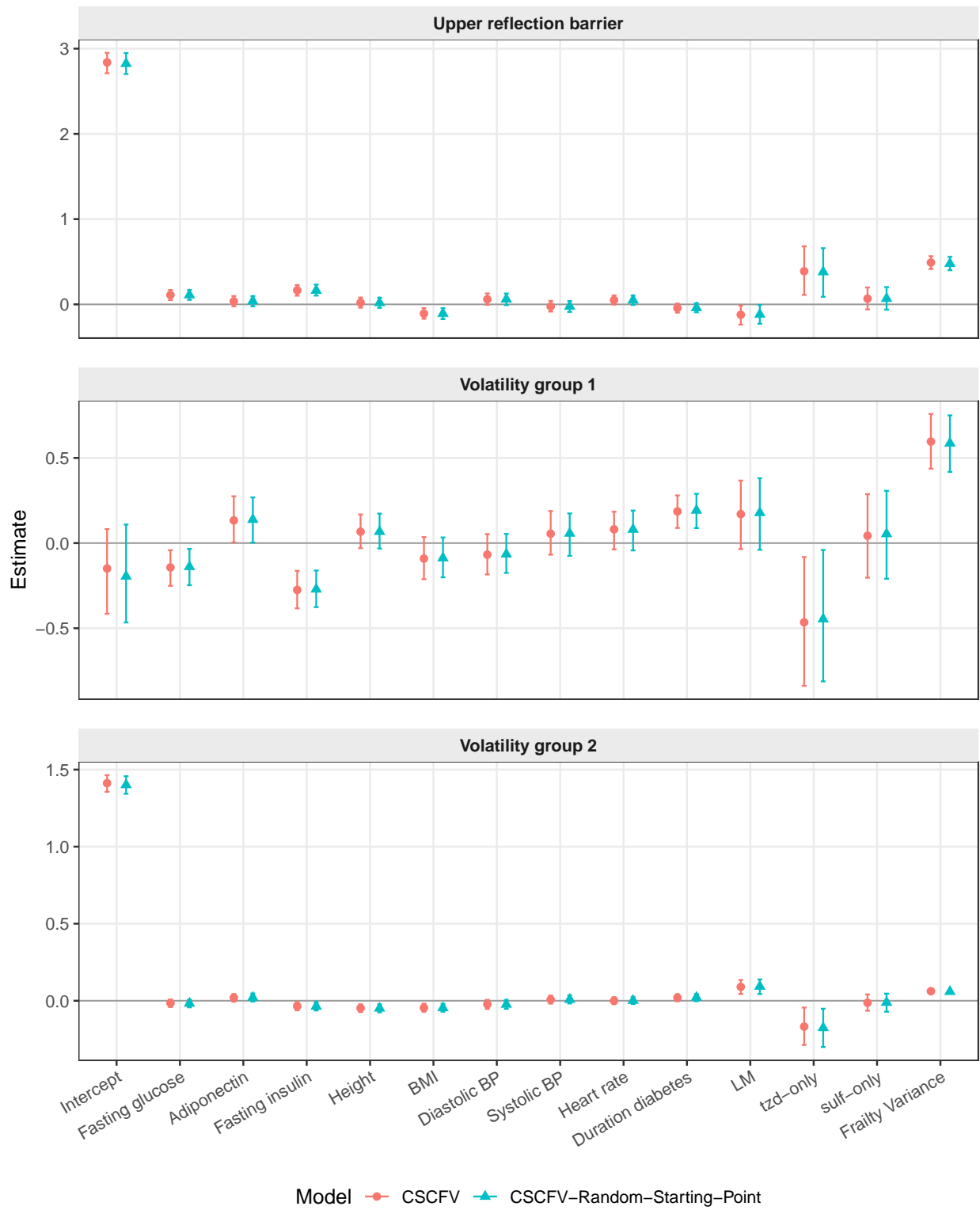


Figure 4: Comparison of covariate effect estimates between the CS-C-FV models with fixed and random starting points.

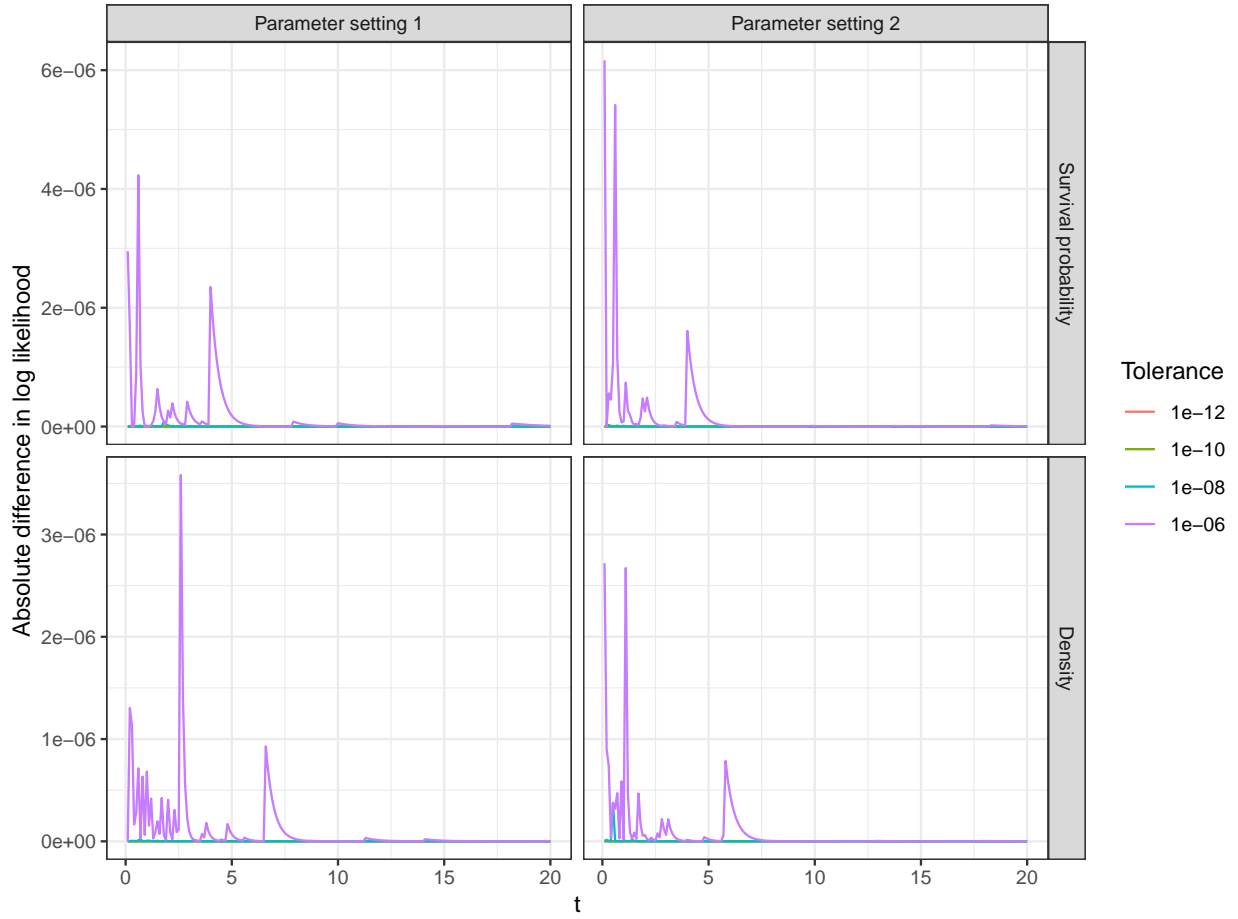


Figure 5: Absolute differences in log-likelihood evaluation for the FHT density and survival probability under different tolerance levels, relative to the practically untruncated reference (tolerance = 0). Results are shown across representative parameter settings and gap times. The parameter settings correspond to  $(x_0, \nu, \kappa, \sigma) = (10, 3.9, 20, 1)$  and  $(10, 3.9, 30, 2)$ .

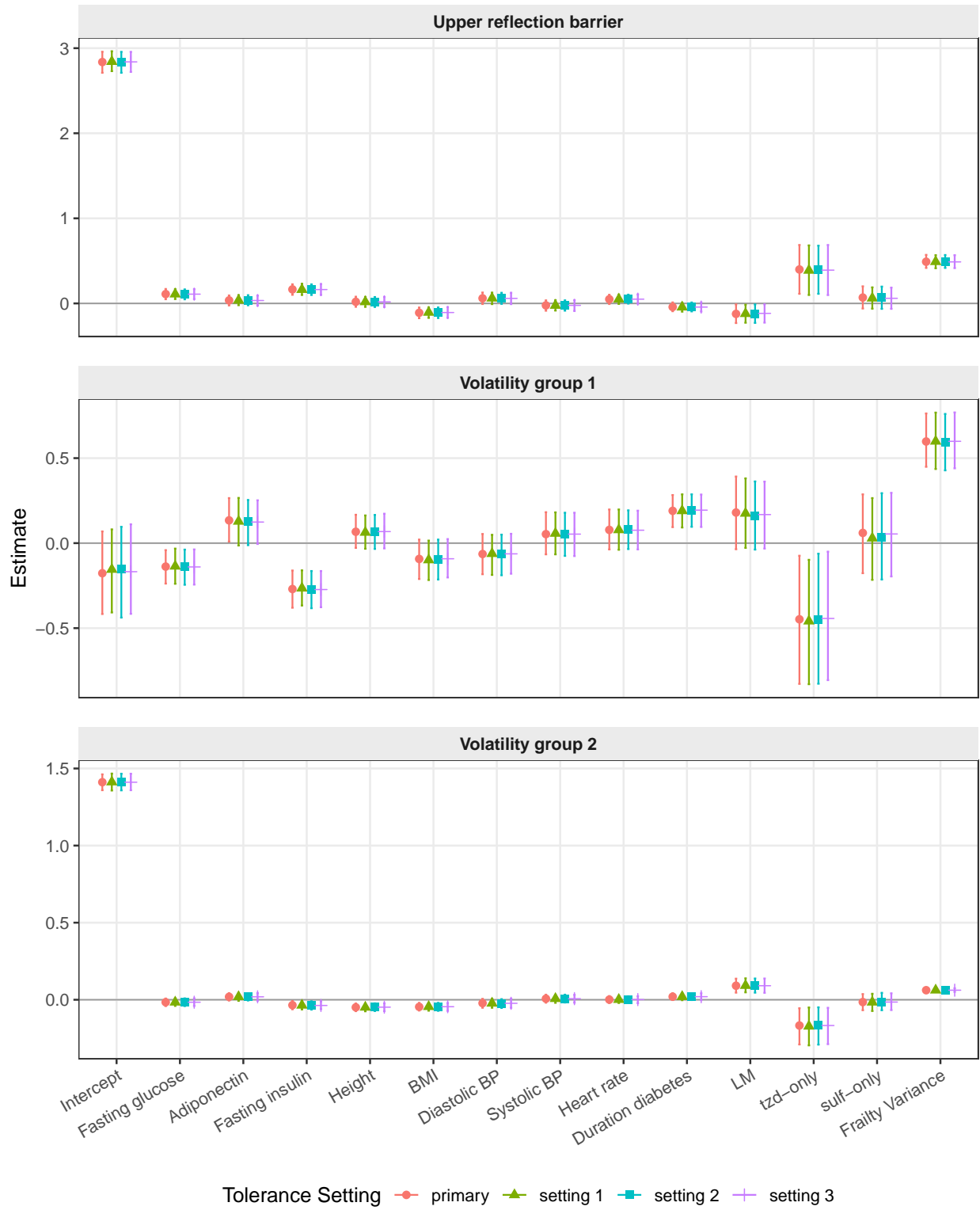


Figure 6: Comparison of parameter estimates from the data analysis under different tolerance levels used in the implementation of the FHT density and distribution functions.

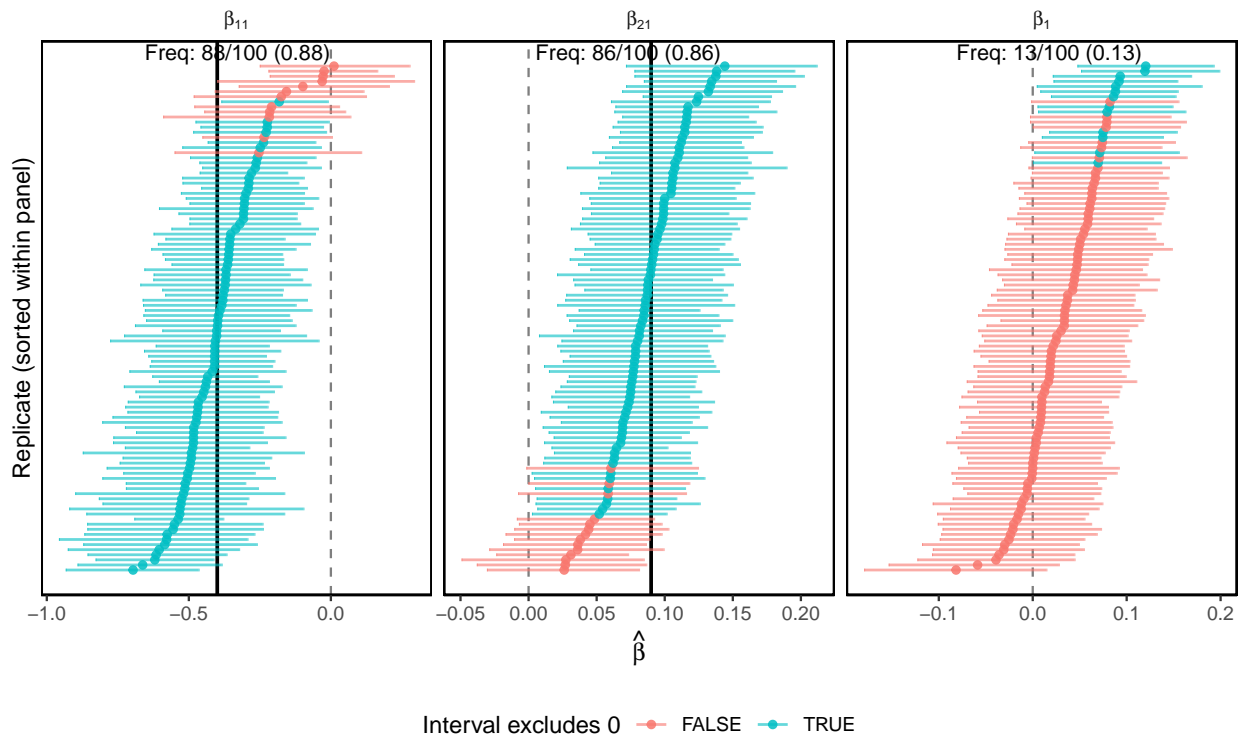


Figure 7: Forest plots for estimation of  $\beta$ s

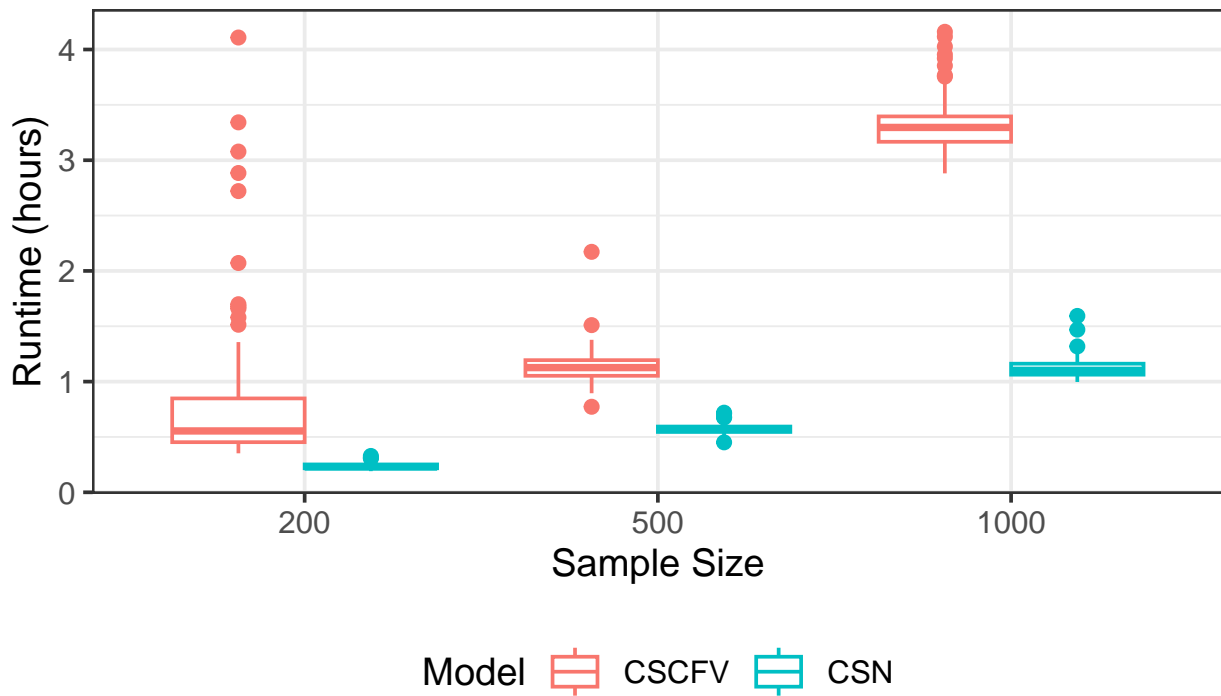


Figure 8: Runtime for estimation of CS-C-FV and CS-N model